Mathematical Biosciences 371 (2024) 109179

Contents lists available at ScienceDirect

Mathematical Biosciences

journal homepage: www.elsevier.com/locate/mbs

Original Research Article

Mathematical generation of data-driven hippocampal CA1 pyramidal neurons and interneurons copies via A-GLIF models for large-scale networks covering the experimental variability range

A. Marasco [a,b,*], C. Tribuzi [a], A. Iuorio [c,d], M. Migliore [b]

[a] Department of Mathematics and Applications, University of Naples Federico II, Naples, Italy
[b] Institute of Biophysics, National Research Council, Palermo, Italy
[c] University of Vienna, Faculty of Mathematics, Vienna, Austria
[d] Department of Engineering, Parthenope University of Naples, Naples, Italy

ARTICLE INFO

Keywords:
Neuronal modeling
Adaptive generalized leaky integrate-and-fire (A-GLIF) models
Hippocampal CA1 pyramidal neurons and interneurons
Neuron copies
EBRAINS platform

ABSTRACT

Efficient and accurate large-scale networks are a fundamental tool in modeling brain areas, to advance our understanding of neuronal dynamics. However, their implementation faces two key issues: computational efficiency and heterogeneity. Computational efficiency is achieved using simplified neurons, whereas there are no practical solutions available to solve the problem of reproducing in a large-scale network the experimentally observed heterogeneity of the intrinsic properties of neurons. This is important, because the use of identical nodes in a network can generate artifacts which can hinder an adequate representation of the properties of a real network.

To this aim, we introduce a mathematical procedure to generate an arbitrary large number of copies of simplified hippocampal CA1 pyramidal neurons and interneurons models, which exhibit the full range of firing dynamics observed in these cells — including adapting, non-adapting and bursting. For this purpose, we rely on a recently published *adaptive generalized leaky integrate-and-fire (A-GLIF)* modeling approach, leveraging on its ability to reproduce the rich set of electrophysiological behaviors of these types of neurons under a variety of different stimulation currents.

The generation procedure is based on a perturbation of model's parameters related to the initial data, firing block, and internal dynamics, and suitably validated against experimental data to ensure that the firing dynamics of any given cell copy remains within the experimental range. A classification procedure confirmed that the firing behavior of most of the pyramidal/interneuron copies was consistent with the experimental data. This approach allows to obtain heterogeneous copies with mathematically controlled firing properties. A full set of heterogeneous neurons composing the CA1 region of a rat hippocampus (approximately 1.2 million neurons), are provided in a database freely available in the *live paper* section of the EBRAINS platform.

By adapting the underlying A-GLIF framework, it will be possible to extend the numerical approach presented here to create, in a mathematically controlled manner, an arbitrarily large number of non-identical copies of cell populations with firing properties related to other brain areas.

1. Introduction

Computational models of multiple brain areas provide an invaluable tool to make significant advances to understand how a brain works, from cognitive functions and dysfunctions to digital twin implementations.

Several techniques have been implemented for these purposes. One of them is to consider the neural dynamics collectively through a mean-field approach, to obtain dimensionality reduction [1–4]. Another well-established strategy relies on the construction of large-scale networks linking the dynamics of individual neurons (e.g. using a morphologically and biophysically accurate implementation [5–7], LIF models [8,9] or the Izhikevich model [10,11]). To obtain a solid representation of a mean-field reduction it is necessary to start from a detailed understanding not only of individual neuron dynamics but also of the network to which they belong [12]. Efficient and accurate large-scale networks hence represent an essential tool to study neural

* Corresponding author at: Department of Mathematics and Applications, University of Naples Federico II, Naples, Italy.
E-mail address: marasco@unina.it (A. Marasco).

https://doi.org/10.1016/j.mbs.2024.109179
Received 24 March 2023; Received in revised form 10 November 2023; Accepted 13 March 2024
Available online 21 March 2024

dynamics. However, in dealing with such structures, two crucial issues arise: computational efficiency and heterogeneity.

Computational efficiency is required to ameliorate the current technical limitations of supercomputer systems, especially in terms of energy, computational, and memory requirements. From this point of view, neuron models (and their networks) that achieve a good compromise between accuracy and computational efficiency are the generalized leaky integrate-and-fire (GLIF) models, complemented by appropriate initial and update conditions (e.g. [13–15]). Extensions of this modeling framework include the extended GLIF (E-GLIF) and the adaptive GLIF (A-GLIF), introduced by Geminiani et al. in [16] and Marasco et al. in [17], respectively. The A-GLIF framework, in particular, allows to obtain better constraints in the model parameters' space, and to obtain a quantitative agreement with the observed number and timing of spikes experimentally observed in 84 CA1 neurons and interneurons in response to a wide range of input currents.

Cells heterogeneity is another important issue. Large-scale neural networks incorporating cell type diversity (due to e.g. intrinsic physiology, morphology, connectivity, and genetic identity) have in fact been proven to strongly influence the emergent properties of neural networks, hence playing a fundamental role in the information processing in the nervous system (see [18] and references therein). While implementing identical neurons in a network is biologically unrealistic [19], the use of non-identical neurons may be analytically and computationally more challenging, although this leads to networks which better reproduce different types of firing behavior, including synchronization [8,11,20–25]. However, virtually all networks of simplified neurons still use identical neurons.

Libraries of different sizes, providing non-identical neuron copies based on available experimental data, have been obtained by either perturbing the intrinsic model parameters of point-neuron models (e.g. [10,18,26,27]) or adding noise to perturb morphological features in such a way to create copies whose firing patterns remains within experimental ranges (e.g. [28–30] and references therein). For accurate morphological and biophysical implementations (e.g. [6,7]), this problem has been solved using cloning procedures able to generate an appropriate number of cells with individual prperties consistent with the experimental variability.

These ex-post approaches do not allow to anticipate the firing behavior of a clone, and this may significantly slow down the process of creating neurons with the proper electrophysiological properties representing, for example, specific sub-populations or distributions.

In this work, we introduce a novel methodology to implement copies representing the different firing dynamics of CA1 neurons and interneurons, by perturbing specific parameters in the A-GLIF model introduced in [17]. We show how it is possible to control the dynamical behavior of the copies and, at the same time, to remain bounded within the experimental range.

The full database of approximately 1.2 million neurons can be found in the *live papers* section of EBRAINS (https://ebrains.eu/service/live-papers/) [31], can be used to arrange the entire neurons population of a rat hippocampal CA1 area. The code can be easily extended to generate an arbitrary larger population, to consider other brain regions.

The paper is structured as follows: in Section 2 we introduce the reference experimental data used to obtain the database, together with the A-GLIF modeling framework used to investigate neurons' dynamics. Moreover, we illustrate the numerical strategy adopted for the classification of any given neuron copy as member of the pyramidal/interneurons classes. In Section 3 we discuss different cloning procedures and the algorithm to generate copies with controlled firing properties. We conclude our work with a discussion of the results and an outline of future research perspectives in Section 4.

2. Materials and methods

2.1. Experimental data

As a reference to implement our procedure, we considered a set of over 500 somatic voltage traces recorded from 84 cells: 58 pyramidal and 26 interneurons, obtained *in vitro* from rat hippocampal CA1 slices [32], in response to somatic constant current injections, from $I_{\text{stim}}^{\text{min}} = 200\,\text{pA}$ to $I_{\text{stim}}^{\text{max}} = 1000\,\text{pA}$. The physiological variability for pyramidal neurons and interneuron is shown in Fig. 1. The 314 traces from pyramidal neurons (Fig. 1, left column) were all classified as *continuous accommodating cells* (cAC); for interneurons (Fig. 1, right column), 54 traces were classified as cAC, 72 traces as *bursting cells* (bAC), and 62 traces as *continuous non-accommodating cells* (cNAC). To better illustrate the different firing behavior within each class, in Fig. 2 we show typical examples of number of spikes as a function of the input current. Note the rather different results, in response to the same input, observed for different cells in both pyramidal cells (Fig. 2, left panel) and interneurons (Fig. 2, right panel).

2.2. The A-GLIF model

2.2.1. Model equations, initial and update conditions

In [17] we introduced the A-GLIF model which aims to describe the evolution, in a subthreshold regime, of the membrane potential V coupled with the adaptation (I_{adap}) and depolarization (I_{dep}) currents as follows:

$$\begin{aligned}
\frac{dV}{dt} &= \frac{1}{C_{\text{m}}}\left[\frac{C_{\text{m}}}{\tau_{\text{m}}}\left(V - E_{\text{L}}\right) - I_{\text{adap}} + I_{\text{dep}} + I_{\text{stim}}\right],\\
\frac{dI_{\text{adap}}}{dt} &= -k_2 I_{\text{adap}} + C_{\text{m}} k_1 k_2 \left(V - E_{\text{L}}\right),\\
\frac{dI_{\text{dep}}}{dt} &= -k_1 I_{\text{dep}},
\end{aligned} \tag{1}$$

where all the parameters are positive, except for the resting potential E_L, and the injected current I_{stim}. Their explanation is given in Table 1.

We assume that the neuron is at rest – i.e., $I_{\text{stim}} = 0$ and $V = E_{\text{L}}$ – for $t < t_{\text{start}}$, where t_{start} represents the first time instant at which the stimulation current is different from zero. Moreover, we denote with I_{th} the *threshold current* above which the neuron starts to fire, i.e. we assume that a spike event occurs when, for $I_{\text{stim}} > I_{\text{th}}$, the potential V reaches the *threshold potential* V_{th}.

Starting from the resting condition, the *first spike* for any $I_{\text{stim}} > I_{\text{th}}$ can be obtained by setting the initial conditions of the Cauchy problem associated to system (1) as follows

$$\begin{aligned}
V(t_{\text{start}}) &= E_{\text{L}},\\
I_{\text{adap}}(t_{\text{start}}) &\equiv I_{\text{adap}}^{\text{start}} = 0,\\
I_{\text{dep}}(t_{\text{start}}) &= I_{\text{dep}}^{\text{start}}(I_{\text{stim}} - I_{\text{th}})\;\theta(I_{\text{stim}} - I_{\text{th}}),
\end{aligned} \tag{2}$$

where $I_{\text{dep}}^{\text{start}}$ is a suitable constant and $\theta(I_{\text{stim}} - I_{\text{th}})$ is the step function defined as

$$\theta(I_{\text{stim}} - I_{\text{th}}) = \begin{cases} 1 & \text{if } I_{\text{stim}} > I_{\text{th}},\\ 0 & \text{if } I_{\text{stim}} \le I_{\text{th}}. \end{cases} \tag{3}$$

Coherently with the LIF framework, the potential V after a spike does not return to the resting value E_{L} but at the *reset potential* V_{r}. Then, for any following spike, the initial conditions of each Cauchy problem associated to (1) are modified according to the following *after-spike update rules*

$$\begin{aligned}
V(t_{\text{spk}}^{+}) &= V_{\text{r}},\\
I_{\text{adap}}(t_{\text{spk}}^{+}) &= I_{\text{adap}}^{0}(t_{\text{spk}}^{+}, I_{\text{stim}}),\\
I_{\text{dep}}(t_{\text{spk}}^{+}) &= I_{\text{dep}}^{0},
\end{aligned} \tag{4}$$

where t_{spk}^{+} is the time instant following the spike time t_{spk}, i.e. $t_{\text{spk}}^{+} = t_{\text{spk}} + \Delta t_{\text{ref}}$, with $\Delta t_{\text{ref}} = 2\,\text{ms}$ defined as the *refractory time*, $I_{\text{adap}}^{0}(t_{\text{spk}}^{+}, I_{\text{stim}})$

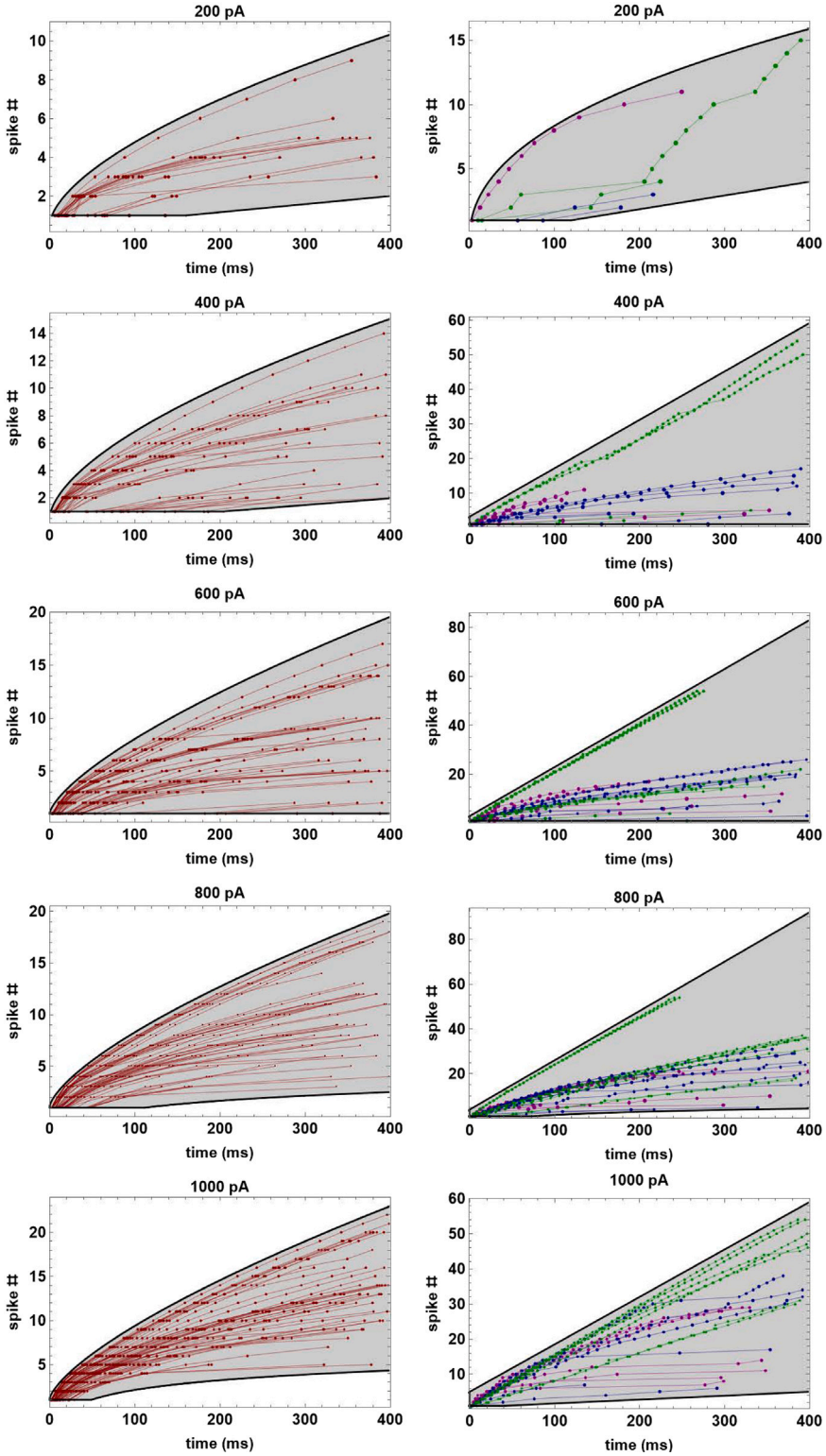

Fig. 1. Reference experimental data and their range of variability. Spike number as a function of spike times for pyramidal neurons (left column, red markers and lines) and CA1 interneurons (right column) classified as cAC (blue markers and lines), bAC (magenta markers and lines), and cNAC (green markers and lines). Gray areas represent the variability regions bounded by the black curves (detailed expression available in the Supplementary information).

is a suitable set of initial values that depend on both the stimulation current I_{stim} and the corresponding spike times, and I^0_{dep} is a constant.

We remark that in Eq. $(1)_1$ the passive current $1/\tau_{\text{m}}\left(V - E_{\text{L}}\right)$ is opposite in sign to the leakage current component of a traditional *leaky integrate-and-fire model* (see [33]). In these models, since all active membrane conductances are ignored, in order to bring the membrane potential V back to its resting value after a perturbation, a passive leakage current $-\left(V - E_{\text{L}}\right)/\tau_{\text{m}}$ around the resting potential E_{L} is adopted, so that in the absence of other currents it will lead to a stable equilibrium. However, in system (1) it has the opposite sign and, should it be the only current, it would lead to an unstable membrane potential equilibrium. Nevertheless, in the proposed model the second term in

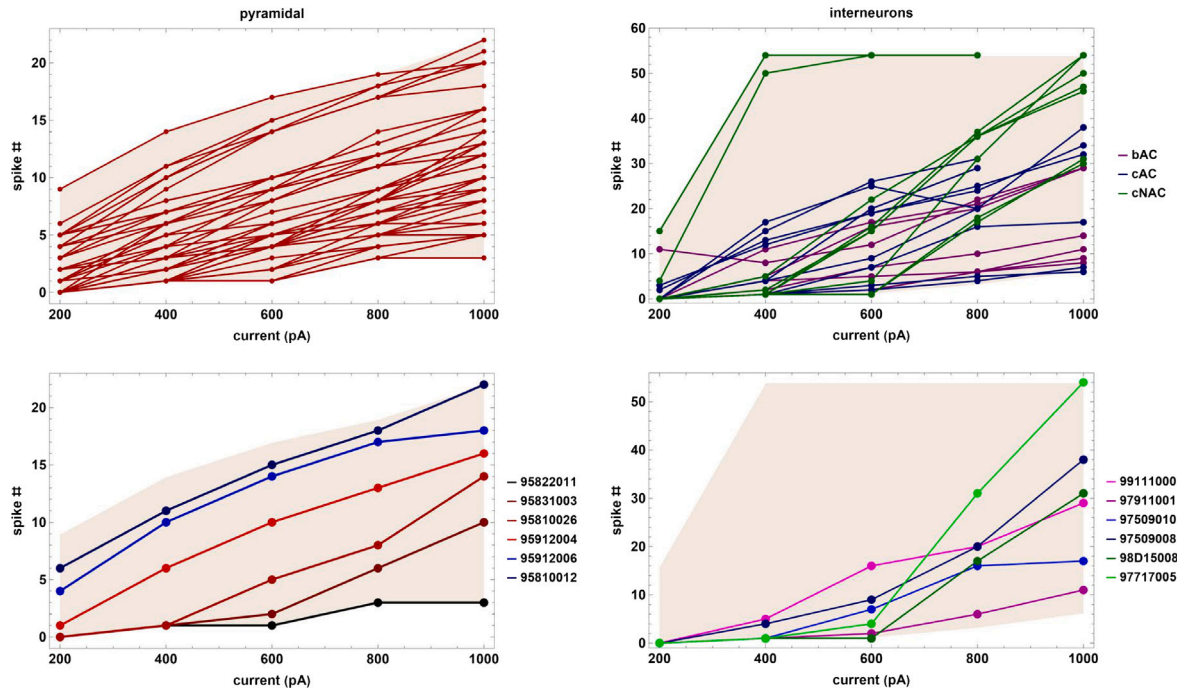

Fig. 2. Number of spikes as a function of the stimulation current. Pyramidal neurons (left column) and interneurons (right column) of type cAC (blue markers and lines), bAC (magenta markers and lines), and cNAC (green markers and lines). The lower panels correspond to typical data for the spike number as a function of the stimulation currents for some pyramidal neurons (left) and interneurons (right).

Table 1
List of parameters appearing in Eq. (1) including their description and measurement unit.

Parameter	Description	UM
E_L	resting potential	mV
V_r	reset potential	mV
V_{th}	threshold potential	mV
Δt_{ref}	refractory interval	ms
I_{stim}	external stimulation current	pA
C_m	membrane capacitance	pF
τ_m	membrane time constant	ms
I_{th}	threshold stimulation current	pA
k_2	I_{adap} decay rate	ms^{-1}
k_1	I_{dep} decay rate	ms^{-1}

the second equation of model (1), contributing to I_{adap}, depending on the setting of model parameters (particularly its coefficient $C_m k_1 k_2$), can balance or even outweigh the effect of the former inverted leakage current term. As we proved in [17], the introduction in Eq. $(1)_1$ of the currents I_{adap} and I_{dep} in addition to the *inverted leakage* current allows us to increase the complexity of the potential dynamics while preserving the linear nature of the model. In particular, the A-GLIF model allows both to accurately reproduce the excitability properties of hippocampal neurons and interneurons and to make the subthreshold dynamics of V more realistic than the one provided by a classical LIF model. For example, in our A-GLIF framework the subthreshold relaxation of V from V_{reset} exhibits monotonicity properties that are in agreement with experimental recordings but are atypical for a classical LIF model (see Fig. 8 in [17] and the insets in Figs. 6, 7, 10 and Supp. Figs. S.2, S.3, S.6).

2.2.2. Nondimensional formulation of the model

Considering the following rescaled variables

$$\tilde{t} = \frac{t}{\tau}, \qquad \tilde{V} = -\frac{V}{E_L}, \qquad \tilde{I}_{adap} = -\frac{I_{adap}}{E_L\, C_m k_1}, \qquad \tilde{I}_{dep} = -\frac{I_{dep}}{E_L\, C_m k_1}, \tag{5}$$

we obtain an equivalent nondimensional version of system (1) (for simplicity, from now on we will omit the tildes)

$$\begin{aligned} \frac{dV}{dt} &= \alpha + \beta(I_{dep} - I_{adap}) + \delta(1+V), \\ \frac{dI_{adap}}{dt} &= 1 - I_{adap} + V, \\ \frac{dI_{dep}}{dt} &= -\beta I_{dep}, \end{aligned} \tag{6}$$

where

$$\alpha = \frac{I_{stim}}{K}, \qquad \beta = \frac{k_1}{k_2}, \qquad \delta = \frac{1}{k_2\,\tau_m}, \qquad \tau = \frac{1}{k_2}, \tag{7}$$

and $K = -C_m\, E_L\, k_2$ is a positive scaling constant.

Similarly, the dimensionless initial conditions (2) and (4) assume the following forms, respectively,

$$V(t_{start}) = -1, \qquad V(t^+_{spk}) = -\frac{V_r}{E_L}, \tag{8a}$$

$$I_{adap}(t_{start}) \equiv I^{start}_{adap} = 0, \qquad I_{adap}(t^+_{spk}) = I^0_{adap}(t^+_{spk}, I_{stim}), \tag{8b}$$

$$I_{dep}(t_{start}) = I^{start}_{dep}(I_{stim} - I_{th})\theta(I_{stim} - I_{th}), \qquad I_{dep}(t^+_{spk}) = I^0_{dep}, \tag{8c}$$

where all time variables have been rescaled by means of $\tau = 1/k_2$.

In [17], assuming a constant stimulation current I_{stim}, we obtained the analytical form of the solutions of the linear system (6) as follows

$$\begin{aligned} V(t) = &- I^0_{adap}\beta\mathcal{H}_1 + I^0_{dep}\frac{\beta\left[(\beta-1)\left(\mathcal{H}_2 - 2e^{\beta(t_0-t)}\right)\right] + \mathcal{H}_1\left[(\beta-1)(\delta+1)+2\beta\right]}{2\left(\beta^2+(\beta-1)\delta\right)} \\ &+ \frac{V^0}{2}\left[(\delta+1)\mathcal{H}_1 + \mathcal{H}_2\right] + \frac{\mathcal{H}_1}{2}\left[\frac{\alpha(\beta-1)}{\beta-\delta} + \alpha + \delta + 1\right] \\ &- \frac{(\mathcal{H}_2-2)(\alpha-\beta+\delta)}{2(\beta-\delta)}, \end{aligned} \tag{9}$$

$$\begin{aligned} I_{adap}(t) = &\frac{1}{2} I^0_{adap}\left[\mathcal{H}_2 - (\delta+1)\mathcal{H}_1\right] + I^0_{dep}\frac{\beta}{2}\left[\frac{2e^{\beta(t_0-t)} + \mathcal{H}_1(2\beta+\delta-1) - \mathcal{H}_2}{\beta^2+(\beta-1)\delta}\right] \\ &+ V^0\mathcal{H}_1 - \frac{\alpha}{2}\left[\frac{(1-\delta)\mathcal{H}_1 + \mathcal{H}_2 - 2}{\beta-\delta}\right] + \mathcal{H}_1, \end{aligned}$$

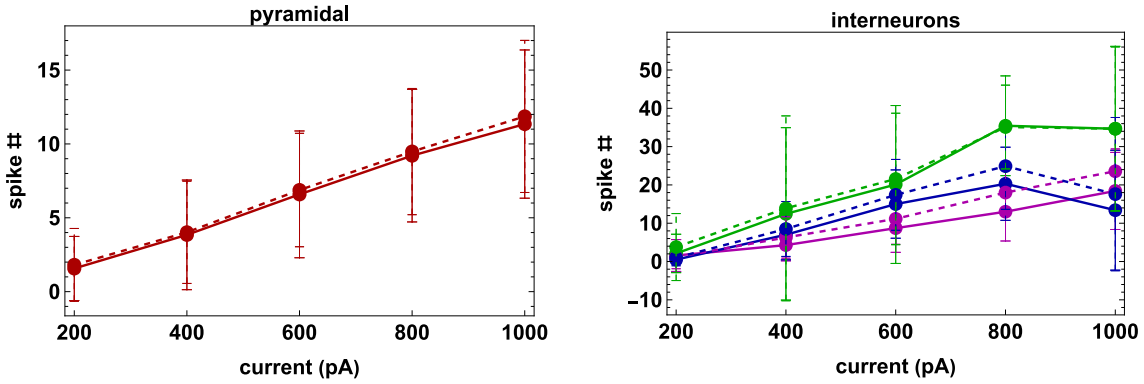

Fig. 3. Comparison between experiments and models. Mean and standard deviation for the number of spikes as a function of the input current for pyramidal neurons (red markers and line) and interneurons cAC (blue markers and lines), bAC (magenta markers and lines), and cNAC (green markers and lines). The continuous and dashed lines represent experimental data and model results, respectively.

$$I_{dep}(t) = I^0_{dep} e^{-\beta(t-t_0)},$$

where the initial data are defined according to (8) as

$$V^0 := V(t_0), \quad I^0_{adap} := I_{adap}(t_0), \quad I^0_{dep} := I_{dep}(t_0), \tag{10}$$

and

$$\mathcal{A} = (\delta+1)^2 - 4\beta, \quad \mathcal{B} = -\frac{1}{2}\left(\sqrt{\mathcal{A}} - \delta + 1\right)(t-t_0), \quad \mathcal{C} = \sqrt{\mathcal{A}}(t-t_0),$$
$$\mathcal{H}_1 = \frac{e^{\mathcal{B}}\left(e^{\mathcal{C}}-1\right)}{\sqrt{\mathcal{A}}}, \quad \mathcal{H}_2 = e^{\mathcal{B}}\left(e^{\mathcal{C}}+1\right). \tag{11}$$

2.2.3. Equilibria, parameter constraints and initial data distributions

Despite the linearity of the equations, the A-GLIF model can reproduce a wide range of physiological firing patterns like bursting, non adapting, and continuous adapting [32], provided that some parameter constraints are imposed and initial data distributions, I^0_{dep} and I^0_{adap}, are suitably chosen. The quantitative agreement between model and experiments is shown in Fig. 3, where we compare findings for both pyramidal neurons and interneurons. Below we report the fundamental results of this analysis; an in-depth investigation can be found in [17].

For $\alpha \neq 0$ or $\beta \neq \delta$, the dynamical system (6) admits the equilibrium

$$E_1 = \left(\frac{\alpha}{\beta-\delta} - 1, \frac{\alpha}{\beta-\delta}, 0\right), \tag{12}$$

that is (globally) asymptotically stable if and only if

$$\delta < \beta \leq \frac{1}{4}(1+\delta)^2 \quad \text{with } 0 < \delta < 1. \tag{13}$$

Moreover, by imposing that the cell does not fire for $0 < I_{stim} < I_{th}$ we obtain

$$\alpha_{th} < \frac{(1+\tilde{V}_{th})(\delta-1)^2}{4}, \quad \frac{\alpha_{th}}{1+\tilde{V}_{th}} + \delta < \beta \leq \frac{1}{4}(\delta+1)^2, \quad 0 < \delta < 1, \tag{14}$$

where $\tilde{V}_{th} = -V_{th}/E_L$ is the nondimensional form of the threshold potential V_{th}, and $\alpha_{th} = I_{th}/K$.

Since $V(t)$ is an increasing function for any positive stimulation current I_{stim}, the initial data I^0_{dep} and I^0_{adap} must satisfy the following condition (see Eq. (8))

$$I^0_{adap} < \frac{\alpha}{\beta} + I^0_{dep} + \frac{\delta}{\beta}(1+V^0) \equiv I^{max}_{adap}, \tag{15}$$

where $V^0 = -1$ or $V^0 = -V_r/E_L$ for the first or after the first spike event, respectively.

In [17] we proved that the $I^0_{adap}(t^+_{spk}, I_{stim})$ distribution for any given cell can be represented by a Monod-type function as follows[1]

$$I^0_{adap}(t^+_{spk}, I_{stim}) := c + \frac{a\, e^{b\, I_{stim}}\,(t^+_{spk} - t_{start})}{\eta + (t^+_{spk} - t_{start})}, \quad \forall I_{stim} \in \left[I^{min}_{stim}, I^{max}_{stim}\right], \tag{16}$$

where a, b, c, η are constants, and t_{start} is the last instant in which $I_{stim} = 0$ or $I_{stim} \leq I_{th}$.

For sake of simplicity, we assume that the function (16) is defined for all $\eta + (t^{first}_{spk} - t_{start}) > 0$, where t^{first}_{spk} is the time of the first spike event for the current I_{stim}, and $\eta \geq 0$. Moreover, Eq. (16) is an increasing monotone function of t when $a\eta > 0$ and decreasing monotone for $a\eta < 0$. The plateau value of I^0_{adap}, defined as

$$P(I_{stim}) := \lim_{t\to+\infty} I^0_{adap}(t, I_{stim}) = c + a e^{bI_{stim}}, \tag{17}$$

is an increasing monotone function of I_{stim} when $a\,b > 0$ and decreasing monotone when $a\,b < 0$.

We note that Eq. (16) defines a sequence of constant ISIs if $a = 0$ and $c \geq 0$ (with I^0_{adap} independent from I_{stim}) or $\eta = 0$ and $c + a e^{bI_{stim}} > 0$ (with I^0_{adap} dependent from I_{stim}). Then, assuming $a \neq 0$ and $\eta > 0$ and imposing that the function (16) is positive for any stimulation current and at any time, we obtain a sequence of nonconstant ISIs by imposing the following additional constraints on parameters a, b and c:

(i) either $a > 0, \quad c \geq 0, \quad \forall b$;
(ii) or $a < 0, \quad b < 0, \quad c \geq -a$.

By simultaneously fitting, for each neuron, the set of I^0_{adap} values for all experimental currents using Eq. (16) (solid curves in Fig. 4), we obtained a function which allows us to predict the spike times of a given neuron for any constant current injection in the interval $[I^{min}_{stim}, I^{max}_{stim}]$.

Several experimental traces show an unexpected block of firing, long before the end of the stimulation at constant current. To reproduce these *firing blocks* for any neuron and any stimulation current I_{stim}, in [17] we implemented a *Monod block procedure* that allowed us to determine the time interval in which the Monod function (16) should be defined. First, we identified the range of currents $[I^I_{block}, I^{II}_{block}]$ such that for $I_{stim} \in [I^I_{block}, I^{II}_{block}]$ a firing block occurs, i.e.

$$t^{last}_{spk}(I_{stim}) + 2\, ISI_{last}(I_{stim}) < T, \tag{18}$$

where t^{last}_{spk} and ISI_{last} are the time and the ISI of the last spike event for the current I_{stim}, respectively, and $[t_{start}, T]$ is the stimulation

[1] We remark that the $I^0_{adap}(t^+_{spk}, I_{stim})$ distributions for all cells provided by the optimization procedure satisfy the constraint (15). However, this constraint could be violated in determining the interpolating function (16) of each cell.

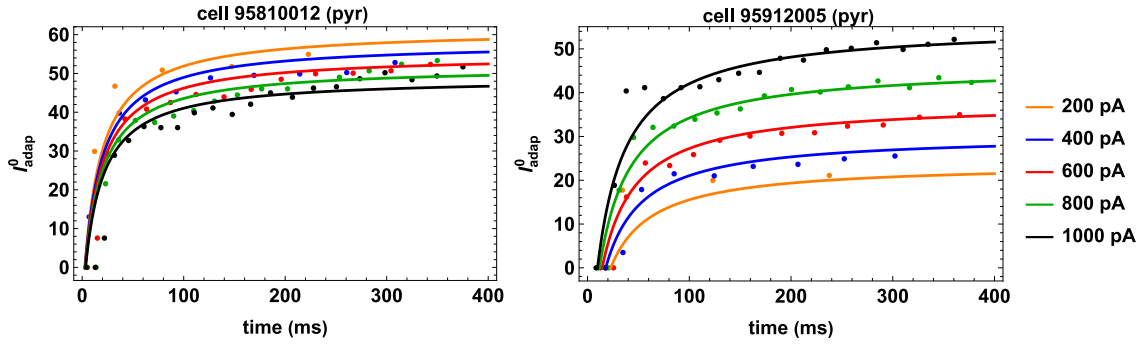

Fig. 4. Monod-type functions. Monod functions (continuous lines) interpolating the initial data distributions $I^0_{adap}(t^+_{spk}, I_{stim})$ (dots) for the pyramidal cells 95810012 (left panel) and 95912005 (right panel).

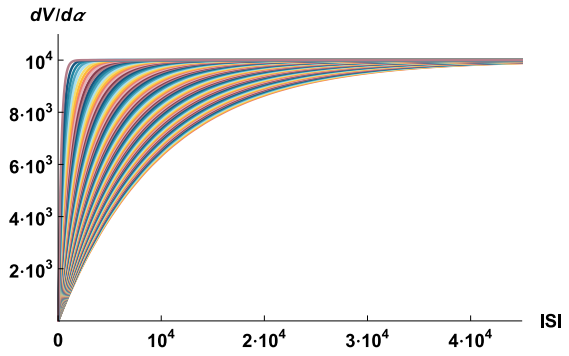

Fig. 5. Plot of the derivative of V respect to α. Plot of the function $\frac{dV}{d\alpha}$ in Eq. (22) as function of $t-t_0$ obtained by varying β and δ within the admissibility ranges defined by conditions (13) with a step of 0.01 for both parameters.

interval. Subsequently, we determined the function

$$t = A_{I,II} I_{stim} + B_{I,II}, \tag{19}$$

where $ISI^I_{last} = ISI_{last}(I^I_{block})$, $ISI^{II}_{last} = ISI_{last}(I^{II}_{block})$, and

$$A_{I,II} = \frac{\left(ISI^{II}_{last} + 2t^{last}_{spk}(I^{II}_{block})\right) - \left(ISI^{I}_{last} + 2t^{last}_{spk}(I^{I}_{block})\right)}{2(I^{II}_{block} - I^{I}_{block})}, \tag{20}$$

$$B_{I,II} = \frac{I^{II}_{block}\left(ISI^{I}_{last} + 2t^{last}_{spk}(I^{I}_{block})\right) - I^{I}_{block}\left(ISI^{II}_{last} + 2t^{last}_{spk}(I^{II}_{block})\right)}{2(I^{II}_{block} - I^{I}_{block})}.$$

Finally, denoting the stimulation current starting from which the firing block does not occur by I_{fire}, the function (19) provides the time interval in which the Monod function (16) is defined as follows

$$\text{for all} \quad I_{stim} \le \frac{I^{II}_{block} + I_{fire}}{2} \equiv I^{inf}_{block} \text{when} \quad I_{fire} > I^{II}_{block}, \tag{21}$$

$$\text{for all} \quad I_{stim} \ge \frac{I^{I}_{block} + I_{fire}}{2} \equiv I^{sup}_{block} \text{when} \quad I_{fire} < I^{I}_{block}.$$

This procedure can be easily generalized when there is only one I_{block} value that satisfies condition (18) by setting $I^I_{block} = I_{block}, I^{II}_{block} = I_{fire}$ when $I_{fire} > I_{block}$; and $I^I_{block} = I_{fire}, I^{II}_{block} = I_{block}$ if $I_{fire} < I_{block}$.

2.2.4. Monotonicity property of V with respect to α

In this section, we show that the function $V(t)$ provided in Eq. (9) is monotonically increasing with respect to α. In particular, we show that the function

$$\frac{dV}{d\alpha} = \frac{2 - \mathcal{H}_1(1 - 2\beta + \delta) - \mathcal{H}_2}{2(\beta - \delta)}, \tag{22}$$

(where the functions $\mathcal{H}_1(t-t_0)$, $\mathcal{H}_2(t-t_0)$ have been defined in (11)) is positive for any $t > t_0$, as also numerically confirmed in Fig. 5.

Equivalently, introducing $T = t - t_0$ we show that $\frac{dV}{d\alpha}(T)$ is strictly positive in T for any $T > 0$. This relies on the fact that:

(i) $\frac{dV}{d\alpha}(0) = 0$
(ii) $\frac{d^2V}{d\alpha\, dT}(0) = 1 > 0$
(iii) $\frac{d^2V}{d\alpha\, dT} \ge 0$ for any β, δ satisfying Eq. (13)
(iv) $\lim_{T\to\infty} \frac{dV}{d\alpha}(T) = \frac{1}{\beta-\delta} > 0$ for any β, δ satisfying Eq. (13).

Conditions (i), (iv) directly follow from Eq. (22). On the other hand, conditions (ii) and (iii) are obtained by rewriting $\frac{d^2V}{d\alpha\, dT}$ in terms of β, δ, and T first

$$\frac{d^2V}{d\alpha\, dT} = \frac{e^{-\frac{1}{2}T\left(\sqrt{\mathcal{A}}-\delta+1\right)}\left(\sqrt{\mathcal{A}} - \delta + \left(\sqrt{\mathcal{A}} + \delta + 1\right)e^{T\sqrt{\mathcal{A}}} - 1\right)}{2\sqrt{\mathcal{A}}}, \tag{23}$$

where $\mathcal{A}$ has been defined in (11).

Substituting $T = 0$ in (23) leads to condition (ii). As for (iii), we observe that the denominator of (23) is always positive under the stability conditions on β and δ given in Eq. (13). On the other hand, the numerator is positive if and only if

$$T\sqrt{\mathcal{A}} \ge \log\left(\frac{4\beta}{\left(\sqrt{\mathcal{A}} + \delta + 1\right)^2}\right). \tag{24}$$

Here, the left-hand side is positive, whereas the right-hand side is negative since the argument of the logarithm is less or equal than 1 for any β, δ satisfying Eq. (13). This inequality is then automatically satisfied, leading to condition (iii).

2.3. Classification analysis

We used the built-in *Mathematica* (ver. 13.01, Wolfram) function `Classify` to perform the classification of the neuron copies as belonging to pyramidal neurons or interneurons classes. Different supervised classifiers together with cross validation procedures, both performed using the internal algorithms of `Classify`, have been implemented. The classifiers that gave the best accuracy with the given dataset was *Gradient Boosted Trees (GBT)*, a machine learning technique for regression and classification problems that produces a prediction model in the form of an ensemble of trees. The trees are trained sequentially to improve the accuracy and robustness of the final model.

3. Results

3.1. Mathematical procedures for models generation

The goal of this section is to describe several mathematical procedures that can be used to generate model neurons with firing properties within the experimental variability range (see Figs. 1–2).

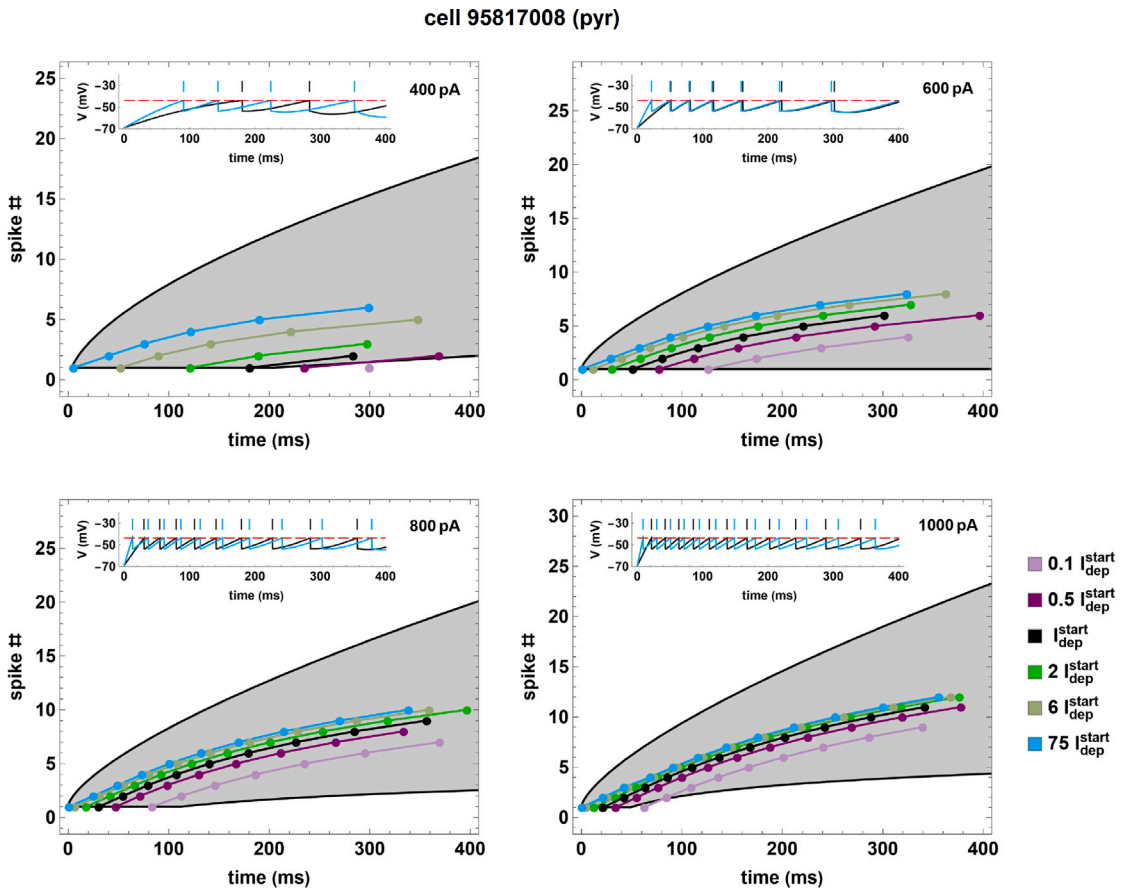

Fig. 6. Spike number as a function time for the pyramidal cell 95817008 (black curves and dots) and for 5 neuron copies (colored curves and dots) obtained by fixing the numerical values of all parameters except $I_{\text{dep}}^{\text{start}}$. For all copies condition (15) is verified. The inset in each panel represents the original simulation compared with the copy corresponding to 75 $I_{\text{dep}}^{\text{start}}$.

3.1.1. *Temporal shift of all spike times*

In this section, we discuss the procedures to delay/anticipate the first spike time and thus to change all other spike times. This can be achieved by modulating $I_{\text{dep}}^{\text{start}}$ and $I_{\text{adap}}^{\text{start}}$ in Eqs. (8), with all the other parameters in Eqs. (7) and (16) fixed.

To this aim, it should be noted that under the constraints (13) the potential V is a decreasing (resp. increasing) function with respect to I_{adap}^0 (resp. I_{dep}^0) when the other initial data are fixed. In fact, we have

$$\frac{dV}{dI_{\text{adap}}^0} = \frac{\beta e^{\frac{1}{2}\sigma(t-t_0)}}{\sqrt{\mathcal{A}}}\left[1 - e^{\sqrt{\mathcal{A}}(t-t_0)}\right] < 0, \tag{25}$$

and it can be numerically proved that (see Supp. Fig. S.1)

$$\frac{dV}{dI_{\text{dep}}^0} > 0. \tag{26}$$

To obtain a different time of first spike, at least one of the values $I_{\text{dep}}^{\text{start}}$ and $I_{\text{adap}}^{\text{start}}$ in Eqs. (8) must be varied. In view of Eqs. (16), modifying the first spike time results in a different distribution for the initial data I_{adap}^0, thus obtaining a different distribution of spike times (see Supp. Figs. S.2 and 6).

Owing to Eqs. (16), (25), and (26), we can modulate the time of both the first and any subsequent spikes by modifying the value of $I_{\text{adap}}^{\text{start}}$ and/or $I_{\text{dep}}^{\text{start}}$. In particular, increasing the values of $I_{\text{adap}}^{\text{start}}$ or $I_{\text{dep}}^{\text{start}}$ will result in increasing or decreasing first spike times, and vice versa, respectively. We note that since I_{adap} is a nonnegative function, in view of Eq. (8b) we can only choose positive values of $I_{\text{adap}}^{\text{start}}$. This leads to an increase in the first spike time compared to the original model (see colored curves and dots in Supp. Fig. S.2). Moreover, in view of Eqs. (15) and (25), for any fixed value of $I_{\text{dep}}^{\text{start}}$, the minimum and maximum values of the first spike time can be obtained by setting the values of $I_{\text{adap}}^{\text{start}}$, respectively, as follows

$$I_{\text{adap}}^{\text{start}} = 0, \qquad I_{\text{adap}}^{\text{start}} = \frac{\alpha}{\beta} + I_{\text{dep}}^{\text{start}}(I_{\text{stim}} - I_{\text{th}})\theta(I_{\text{stim}} - I_{\text{th}}). \tag{27}$$

and, consequently, by setting $I_{\text{adap}}^{\text{start}} \in \left(0, \frac{\alpha}{\beta} + I_{\text{dep}}^{\text{start}}(I_{\text{stim}} - I_{\text{th}})\theta(I_{\text{stim}} - I_{\text{th}})\right)$ we can modify the time of all spikes including the first one (see Supp. Fig. S.2).

Similarly, we can modify the time of the first spike by choosing a different value for $I_{\text{dep}}^{\text{start}}$ (see Fig. 6). In particular, in view of Eqs. (15) and (26), for any fixed value of $I_{\text{adap}}^{\text{start}}$, we can choose arbitrary positive values for $I_{\text{dep}}^{\text{start}}$ provided that condition (15) is satisfied. This leads to an early or late first spike time depending on whether $I_{\text{dep}}^{\text{start}}$ is smaller or larger than the corresponding value in the original model, respectively (see colored curves and dots in Fig. 6).

The above results show that all the spike times can be modulated in a predictable way by choosing different values of $I_{\text{dep}}^{\text{start}}$ and/or $I_{\text{adap}}^{\text{start}}$, provided that condition (15) is satisfied.

3.1.2. *Temporal shift of all spike times except the first one*

In this section, we examine mathematical procedures allowing to delay/anticipate all spike times except the first one. This can be obtained in two ways: either modifying I_{dep}^0 or modifying the parameters c and η of the Monod function (16).

In the first case, considering Eq. (26) and fixing the initial values of V^0 and I_{adap}^0, we have that increasing values of I_{dep}^0 result in decreasing $ISIs$, and vice versa (see Fig. 7). We remark that shifting the first spike time automatically induces a shift of all the subsequent spike times.

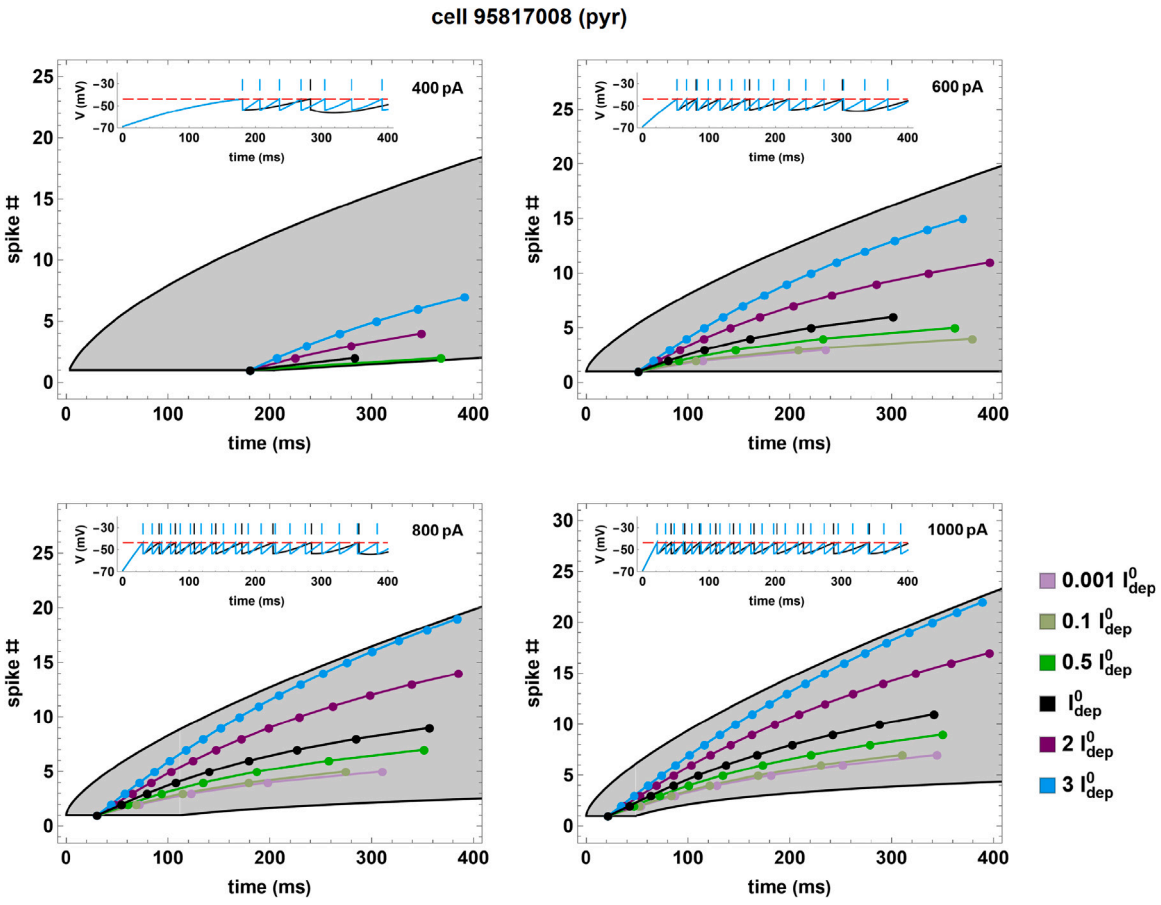

Fig. 7. Spike number as a function of time for the pyramidal cell 95817008 (black curves and dots) and for 5 neuron copies (colored curves and dots) obtained by fixing the numerical values of all parameters except I^0_{dep}. For all copies condition (15) is verified. The inset in each panel represents the original simulation compared with the copy corresponding to the $3\ I^0_{\text{dep}}$.

This in turn modifies the values of I^0_{adap} given by the Monod function (16); such effect, however, mainly depends on the monotonicity properties of the Monod function and of the potential V with respect to I^0_{adap}. In the second case, recalling Eq. (16), we have

$$\frac{d\,I^0_{\text{adap}}}{d\,\eta} = -\frac{a e^{bI_{\text{stim}}}(t^+_{\text{spk}} - t_{\text{start}})}{\left[\eta + (t^+_{\text{spk}} - t_{\text{start}})\right]^2}, \tag{28}$$

i.e. the function I^0_{adap} is decreasing or increasing with respect to η when $a > 0$ or $a < 0$, respectively. Consequently, if we fix the initial values of V^0 and I^0_{dep} and the parameters a, b, c, increasing values of η will result in increasing $ISIs$ when $a < 0$ and in decreasing $ISIs$ when $a > 0$ (see Supp. Fig. S.3). It should be noted that the Monod functions (16) obtained by modifying the parameter η have the same plateau value $c + ae^{bI_{\text{stim}}}$ (see Supp. Fig. S.4); this implies that condition (15) is automatically satisfied.

In contrast, a change in the c parameter results in a translation of the Monod function along the y-axis, and therefore in a different value of the plateau (see Supp. Fig. S.5). However, in this case to satisfy condition (15) for all injected currents I_{stim} it is sufficient to perturb c as follows

$$c' = c + \varepsilon_c: \qquad \varepsilon_c \in \left(-c,\ \frac{\alpha}{\beta} + I^0_{\text{dep}} + \frac{\delta}{\beta}(1 + V^0) - \left(c + ae^{bI_{\text{stim}}}\right)\right). \tag{29}$$

In Supp. Fig. S.6 we show an example illustrating the effect of this perturbation.

3.1.3. Changing the number of spikes

The goal of this section is to define mathematical procedures leading to an increase/decrease in the total number of spikes. This can be achieved either by modifying the time interval in which the Monod function (16) is defined (i.e. when a firing block occurs in response to a stimulation current I_{stim}) or by varying the nondimensional parameter α in Eq. (7).

The first procedure is realized by modifying the coefficients $A_{I,II}, B_{I,II}$ in (19). In particular, by introducing in (19) the perturbed parameters

$$A'_{I,II} = A_{I,II} + \varepsilon_A, \qquad B'_{I,II} = B_{I,II} + \varepsilon_B, \tag{30}$$

we obtain a firing block in the stimulation interval $[t_{\text{start}}, T]$ and in response to the stimulation current I_{stim} at the time

$$t'_{\text{block}}(I_{\text{stim}}) = t_{\text{block}}(I_{\text{stim}}) + \left(\varepsilon_A I_{\text{stim}} + \varepsilon_B\right), \tag{31}$$

where t_{block} is the time in which the firing block occurs for the original model in response to the stimulation current I_{stim}, i.e.

$$t_{\text{block}}(I_{\text{stim}}) = A_{I,II} I_{\text{stim}} + B_{I,II}, \tag{32}$$

if and only if $\varepsilon_A, \varepsilon_B$ are chosen such that

$$t^{\text{first}}_{\text{spk}} - t_{\text{block}} < \varepsilon_A I_{\text{stim}} + \varepsilon_B < T - t_{\text{block}}, \tag{33}$$

where $t^{\text{first}}_{\text{spk}}$ is the time of the first spike in response to the stimulation current I_{stim}.

In particular, we have

- $t'_{\text{block}} < t_{\text{block}}$ when $t^{\text{first}}_{\text{spk}} - t_{\text{block}} < \varepsilon_A I_{\text{stim}} + \varepsilon_B < 0$;
- $t'_{\text{block}} > t_{\text{block}}$ when $0 < \varepsilon_A I_{\text{stim}} + \varepsilon_B < T - t_{\text{block}}$.

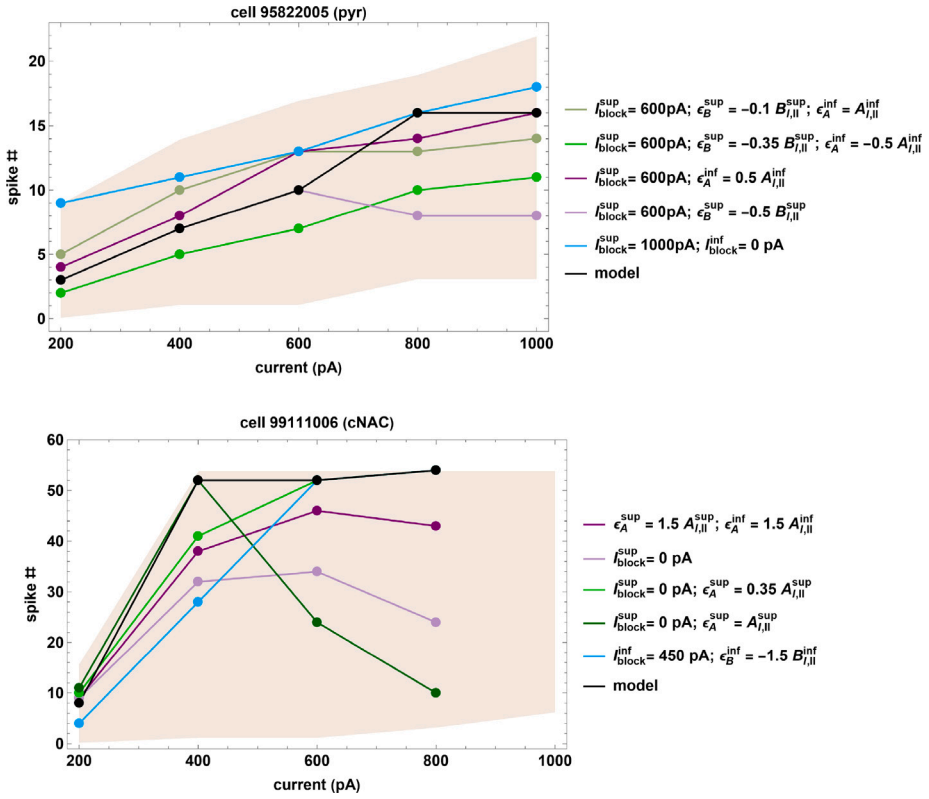

Fig. 8. Effects of firing block perturbation. The two panels show the result of obtained using different combinations of firing block parameters, starting from two original optimizations (cell 95822005 and 99111006).

We note that, with this approach, the range of currents in which the firing block occurs remains unchanged. However, in the copy generation procedure it is also possible to eliminate one or both firing block effects or to modify the value of I^{sup}_{block} and I^{inf}_{block} in Eq. (21) (see Fig. 8). The perturbation of each type of block (superior or inferior) is characterized by the triplet $(I^{sup}_{block}, \epsilon^{sup}_A, \epsilon^{sup}_B,)$ or $(I^{inf}_{block}, \epsilon^{inf}_A, \epsilon^{inf}_B)$, respectively. In particular, since the spike times are not affected by such perturbation, plots as the ones shown in Fig. 8 (consisting in variations of Input/Output (I/O) curves) help us emphasizing how the firing block perturbations illustrated above affect the number of spikes for different stimulation currents. An analogous variation in the I/O behavior of a given neuron is shown in Fig. 9. There, we present the results obtained by changing, one parameter at the time, the overall shape of the excitability curve in such a way to: (1) cover the entire experimental variability range (shaded area in Fig. 9), starting from the optimization of a given experimental neuron (Fig. 9, black in top panel), (2) invert the I/O response (Fig. 9, middle panel), or (3) change the I/O curvature (Fig. 9, bottom panel). Similar results (see Suppl. Fig. S.7) can be obtained using several other parameters' perturbation.

In Fig. 11 we compare the spike number as a function of the spike times for the A-GLIF model of the pyramidal cell 95817008 with those obtained for each of the 90 neuron copies. Note the large variability, in response to the same input, observed for the neuron copies.

Another way to change the total number of spikes is modifying the nondimensional parameter α while keeping β, δ, and τ constant (see Eq. (7); we recall that K is a positive scaling constant defined as $K = -C_m\, E_L\, k_2$). The variations on α is therefore going to be interpreted as variations in the dimensional parameters C_m (whose values are derived from optimization procedures), whereas $\tilde{V}_{th}$ and E_L are considered constant due to their biophysical meaning. We use the superscript ^{n} and ^{o} to indicate the "*new*" and "*old* " value (for the neuron copies) of the corresponding parameter, respectively.

In particular, we consider $C^n_m = p\, C^o_m$ with $p \neq 1$ being a positive parameter, whereas k_2, k_1, and τ_m maintain the same value. This implies $\alpha^n = \frac{\alpha^o}{p}$, while β, δ, and τ remain unchanged. Consequently, the stability conditions (13) are identically satisfied. An important consequence of considering the updated parameter $\alpha^n = \frac{\alpha^o}{p}$ is that the threshold of the stimulation current I_{th} must also change accordingly by introducing $I^n_{th} = p\, I^o_{th}$. We provide here an example for sake of clarity. Let us consider a neuron satisfying $I^o_{th} = 300\,\text{pA}$; this implies that when the neuron is stimulated with a current $I_{stim} = 200\,\text{pA}$ it will not fire, whereas for $I_{stim} = 400\,\text{pA}$ the number of spikes will be non-zero – e.g., let us suppose it will be equal to 4. If we create a copy of such neuron with $p = 1/2$ (while leaving the other parameters and initial data unaffected), we have that $\alpha^n = \frac{\alpha^o}{p} > \alpha^o$. Since the potential V is increasing with respect to α (see Section 2.2.4), we have that the neuron copy will produce more spikes than the original one. In particular, when $I_{stim} = 200\,\text{pA}$, the copy will behave as the original neuron behaved for $\frac{I_{stim}}{p} = 400\,\text{pA}$, i.e. will produce 4 spikes. Therefore, the new threshold stimulation current cannot be still considered to be equal to 300 pA, and will have to be decreased proportionally to p as $I^n_{th} = p\, I^o_{th}$ – which is equal to 150 pA. This assumption on I^n_{th} ensures that the condition in Eq. (14) is automatically satisfied for the neuron copy both for any p, since $\alpha^n_{th} = \frac{I^n_{th}}{K^n} = \frac{p\, I^n_{th}}{p\, K^o} = \frac{I^n_{th}}{K^o} = \alpha^o_{th}$.

We can therefore summarize the effects produced by considering neuron copies with $p < 1$ and $p > 1$ as follows (see Fig. 10 for an example):

1. for $p < 1$ we have $\alpha^n > \alpha^o$ and $I^n_{th} < I^o_{th}$. We hence have that the new initial condition on the first interval (defined in Eq. (2)) $I^n_{dep}(t_{start}) = I^{start}_{dep}(I_{stim} - I^n_{th})\,\theta(I_{stim} - I^n_{th})$ is greater than $I^o_{dep}(t_{start})$.

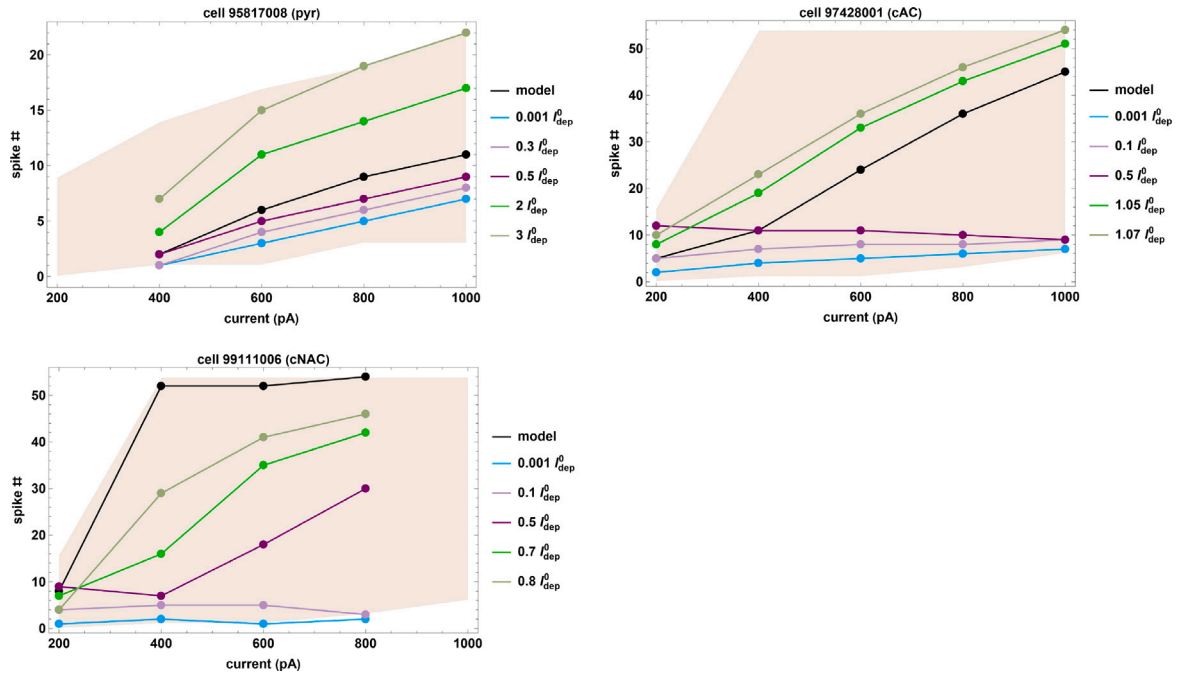

Fig. 9. Number of spikes as a function of the input current. Number of spikes as a function of different constant currents for a pyramidal neuron (top left, black curves and dots), a cAC interneuron (top right, black curves and dots), and a cNAC interneuron (bottom, black curves and dots). Data related to copies obtained by fixing all parameters except for I^0_{dep} are shown via colored curves and dots.

The fact that the potential V is a monotonically increasing function w.r.t. both I^0_{dep} and α (see Section 2.2.4) implies that neuron copies constructed with $p < 1$ always exhibit more spikes than the original neuron.

2. for $p > 1$ we have $\alpha^n < \alpha^o$ and $I^n_{th}(t_{start}) > I^o_{th}(t_{start})$. Therefore, we obtain that here $I^n_{dep} < I^o_{dep}$. The abovementioned monotonicity properties of V w.r.t. both I^0_{dep} and α imply that, in this case, neuron copies constructed with $p > 1$ always exhibit less spikes than the original neuron.

Finally, we note that the parameter τ also affects the spiking dynamics, but only on the nondimensional level, since it only influences the nondimensional time scalings (see Supplementary Materials).

The overall conceptual results of Section 3.1.1– 3.1.3 are summarized in Table 2, where we report a qualitative description of the effects obtained by perturbing different parameters. Additionally, Fig. 11 and Supp. Fig. S.8 provide 90 and 108 neuron copies, respectively, obtained by implementing all parameter variations described in Table 2.

3.2. Numerical implementation of the generation procedure

The aim of this section is to illustrate the numerical procedures leading to *(i)* the generation of neuron copies, and *(ii)* the classification of the dataset of neuron copies into the learned classes pyramidal neurons (pyr) and interneurons (int). As a result of the above numerical procedures, we obtained two downloadable databases, as summarized in Figs. 12 and 14.

3.2.1. Generation of neuron copies

In line with the investigation carried out in Section 3.1, copies of pyramidal neurons and interneurons are generated starting from the optimized values of the following 12 parameters[2]

$$\max I^{start}_{adap},\ I^{start}_{dep},\ I^0_{dep},\ \eta,\ c,\ (I^{sup}_{block}, \varepsilon^{sup}_A, \varepsilon^{sup}_B),\ (I^{inf}_{block}, \varepsilon^{inf}_A, \varepsilon^{inf}_B),\ \alpha \tag{34}$$

via an iterative procedure, where the input value of each parameter is altered by considering a new, rescaled value based on an admissible scaling factor contained in a suitable list of variable size.

A neuron copy is considered admissible if and only if the resulting spike times at each constant stimulation current fall within the corresponding experimental region as represented in Fig. 1 (see Supporting information). Therefore, a validation procedure is run during the copies generation in order to dismiss those for which this requirement does not hold. In this procedure, the set of parameters used for the copy generation is discarded as soon as the numerical spike times, for one or more stimulation currents, lie outside the region defined by experimental data.

In the case of parameters $\max I^{start}_{adap}$ and I^{start}_{dep} it is possible to perform an *a priori* validation study based on the experimental range of first spike time at each current in order to identify ranges of variability for the corresponding scaling factors. This procedure (described into the Supplementary information) allows to reduce the number of dismissed copies resulting from the validation procedure described above, that must be executed nevertheless.

A schematic representation of the implementation procedure is outlined in Fig. 12. Experimental data[3] and optimized parameter values for 84 pyramidal neurons and interneurons (identified by a neuron ID) are stored into a JSON file in a database like structure designed to efficiently retrieve data necessary to calculation. For each parameter in Eq. (34) here generically defined as Γ_i, $i = 1, \dots, 12$, suitable lists ω_i of scaling factors $h_{i,j}$ are defined as

$$\omega_i := \left\{h_{i,j},\ j = 1, \dots, |\omega_i|\right\}.$$

The validation procedure described above will allow to select the admissible coefficients $h_{i,j}$, i.e. the scaling factors for which the new, rescaled parameter $h_{i,j}\Gamma_i$ satisfies the admissibility constraints. We note that for $h_{1,j} = 0$, and $h_{i,j} = 1$ for $i \neq 1$ we retrieve the value of the parameter Γ_i corresponding to the reference neuron from which the

[2] We recall that the perturbations of the parameter α automatically lead to modifying the value of the stimulation current I_{th} (see Section 3.1.3).

[3] The parameter values of E_L, V_r, V_{th} as well as the spike times at any constant currents.

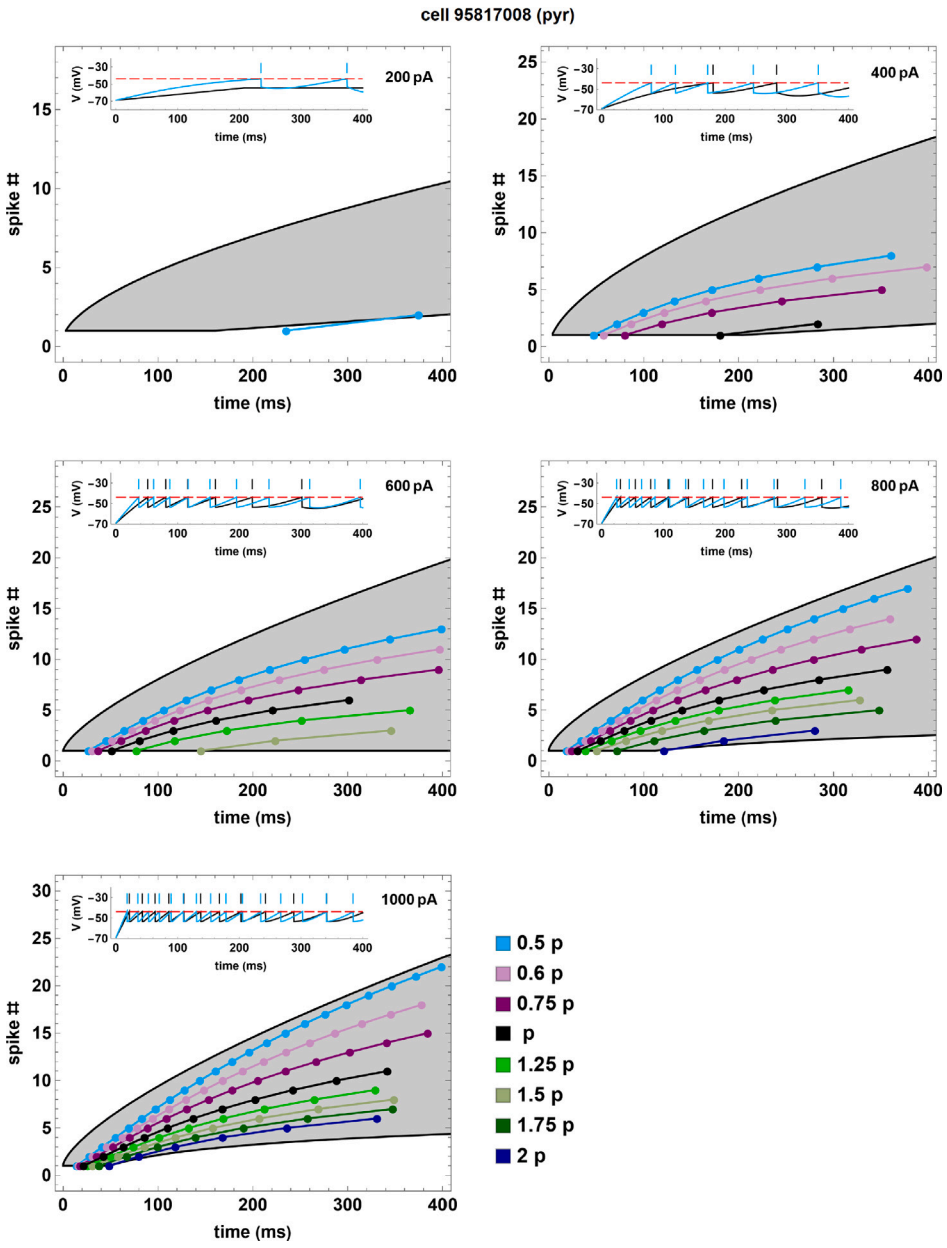

Fig. 10. Spike number as a function of time for the pyramidal cell 95817008 (black curves and dots) and for 7 neuron copies (colored curves and dots) obtained by fixing all parameters except for α. The inset in each panel represents the original simulation compared with the copy corresponding to 0.5 p.

copies are derived. The number of copies generated depends on the number of admissible scaling factors considered for each parameter, up to a maximum of $N := \prod_{i=1}^{12} |\omega_i|$. Within these 12 nested for-loops, the A-GLIF simulations and the validation procedure described above are performed: this finally leads to set the parameters for $M \leq N$ admissible copies which are then saved together with simulated spiking times into an analogous JSON data structure.

Fig. 13 shows a snapshot of the user interface for entering the required information (neuron type and the number of neuron copies) and to visualize the resultant plots of the spike number as a function of the time for the neuron copies. All generated data can be downloaded as a JSON file.

3.2.2. Classification of the neuron copies

In this section, we illustrate the classification procedure to confirm whether the overall firing behavior of a neuron copy falls into the physiological variability of the pyramidal or the interneuron cells. To this end, we characterized the neuronal activity of the cells using the following current-dependent measures for each neuron and trace obtained in response to a constant stimulation current I_{stim}

$$t_{\text{spk}}^{\text{first}}, \quad t_{\text{spk}}^{\text{last}}, \quad n_{\text{tot}}, \quad \text{ISI}_{\text{min}}, \quad \text{ISI}_{\text{max}}, \quad \text{ISI}_{\text{mean}}, \quad \text{ISI}_{\text{SD}}, \tag{35}$$

where $t_{\text{spk}}^{\text{first}}$ and $t_{\text{spk}}^{\text{last}}$ are the times of the first and the last spike, n_{tot} is the total number of spikes; $\text{ISI}_{\text{min}}, \text{ISI}_{\text{max}}, \text{ISI}_{\text{mean}}, \text{ISI}_{\text{SD}}$ are the minimum, maximum, mean and standard deviation values of the ISIs sequence, respectively. Then, we created a binary labeled training dataset (pyr and int) to identify the somatic activity for each of the 58 pyramidal neurons and 26 interneurons using the seven features defined in Eq. (35) obtained by varying the stimulation current from 200pA to 1000pA with a step of 200pA. Hence, all the available experimental data was used as a training set to classify each neuron copy as belonging to pyr neurons or int classes. However, training the GBT classifier with these dataset resulted in a relatively low accuracy performance (about 76.85%) due to both the size imbalance of the two datasets and the

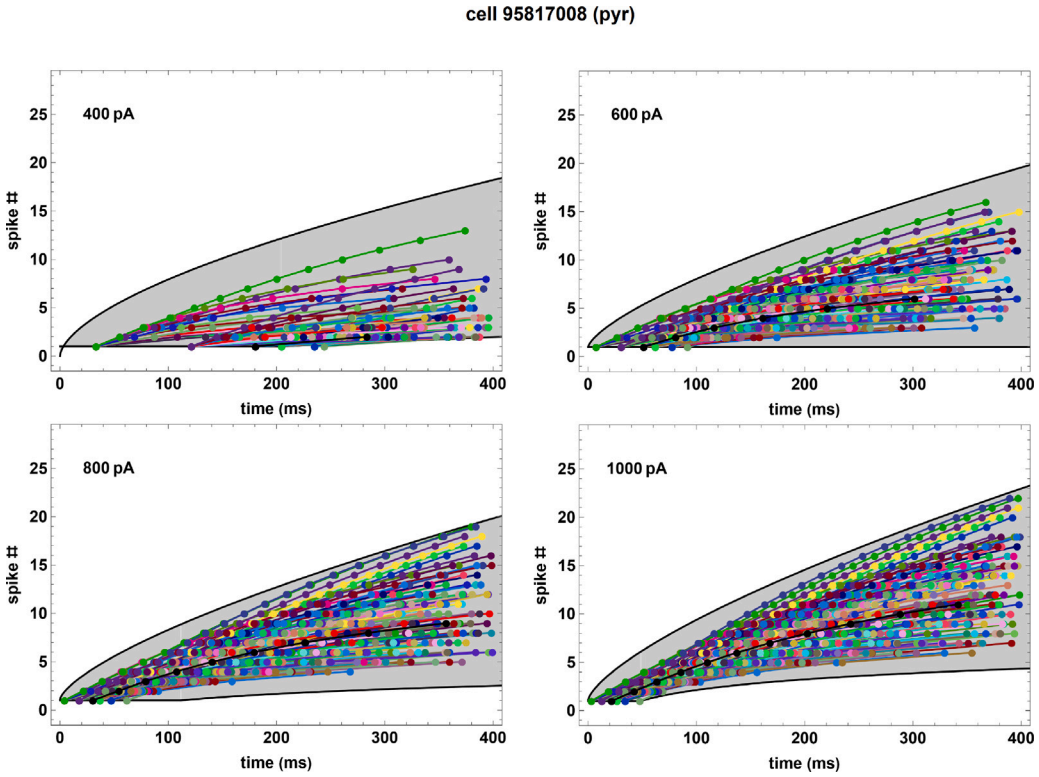

Fig. 11. Spike number as a function of the spike times for the pyramidal cell 95817008 (black curves and dots) and for 90 neuron copies (colored curves and dots) obtained from it by fixing the numerical values of $I_{\text{adap}}^{\text{start}}$ and c and varying the other parameters as follows: $h\, I_{\text{dep}}^{\text{start}}$ where $h = 0.5, 0.75, 1, 2, 10$; $m\, I_{\text{dep}}^{0}$ where $m = 0.1, 0.25, 0.5, 1, 1.5, 2$; $n\,\eta$ where $n = 0.75, 1, 2$. The original model is obtained by setting $h = m = n = 1$ (black curves and dots).

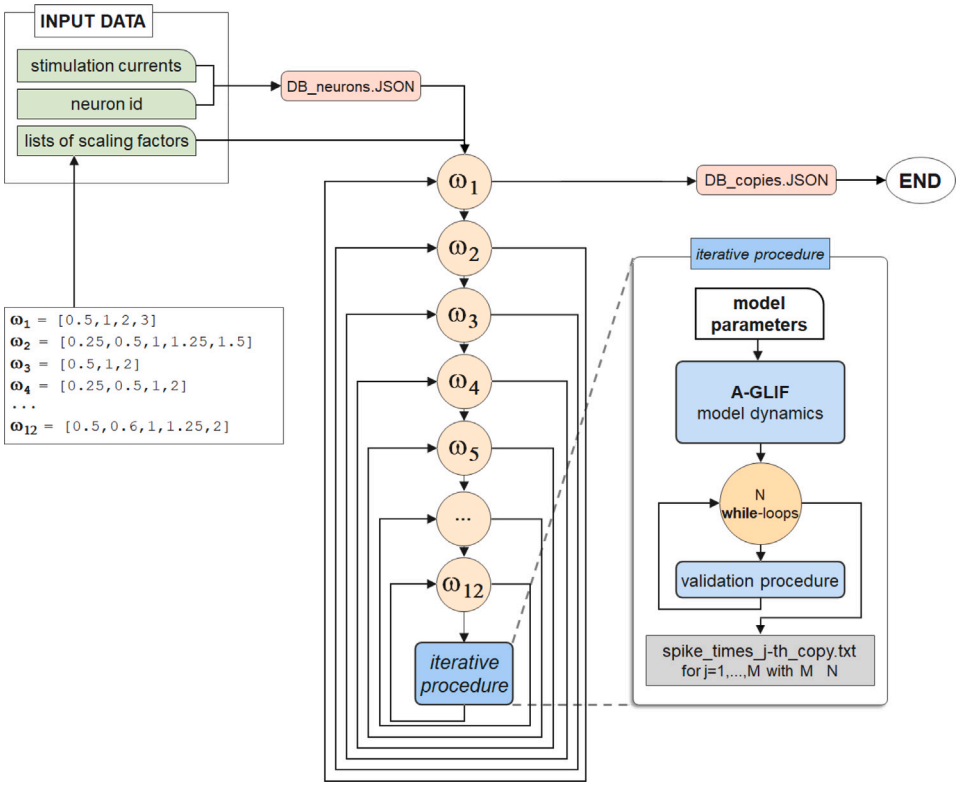

Fig. 12. Flow-chart illustration of the numerical implementation for the generation of a database of neuron copies. Here the sets ω_i, $i = 1, \ldots, 12$ represent the lists of scaling factors leading to modified values of the corresponding parameter Γ_i, representing a generic parameter among the ones in Eq. (34). The initial file `DB_neurons_JSON` containing information about experimental and optimized pyramidal neurons and interneurons is then fed into 12 nested for-loops and, after an A-GLIF simulation and a validation procedure, leads to a new file `DB_copies_JSON` containing information about parameter values and simulated spike times for the generated M admissible copies.

Table 2
Summary of the possible variations in the copies firing dynamics linked to the mathematical procedure for each effect as illustrated in Sections 3.1.1-3.1.3.

Effect	Parameter variation
Temporal shift of all spike times	
Delay the first spike time and changes all other spike times	Increase $I_{\text{adap}}^{\text{start}}$
Anticipate the first spike time and changes all other spike times	Increase $I_{\text{dep}}^{\text{start}}$
Temporal shift of all spike times except the first one	
Anticipate all but the first spike time	Increase I_{dep}^{0}
Delay all but the first spike time	Increase c
Delay/anticipate all but the first spike time if $a > 0$ or $a < 0$, respectively	Increase η
Change in number of spikes	
Generate more/less spikes	Positive/negative values of $\epsilon_A I_{\text{stim}} + \epsilon_B$ for any I_{stim}
Increase the total number of spikes	Increase α ($\Rightarrow$ decrease I_{th})

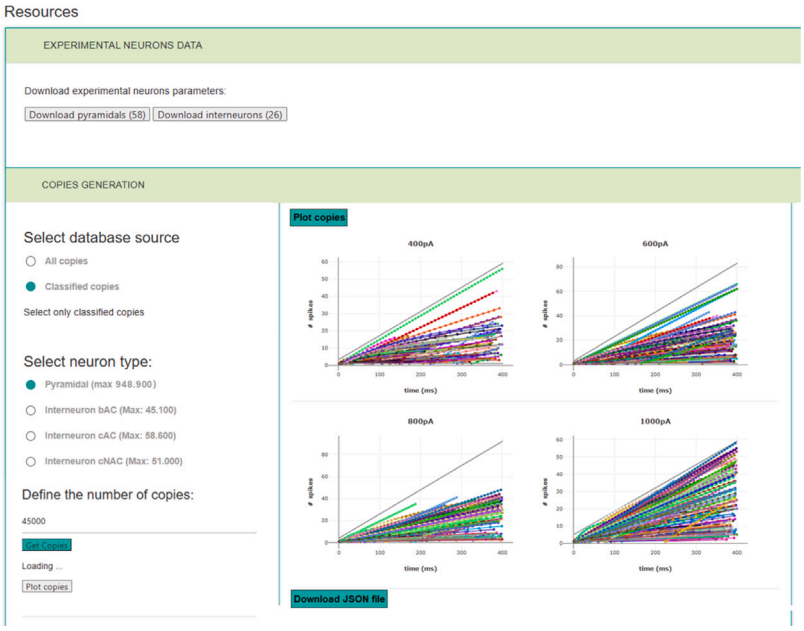

Fig. 13. Copies generation frontend. The user can select the neuron type and set the number of neuron copies. By clicking on *Plot copies* and *Download JSON file* the user can visualize the plots of the spike number as a function of the time for the neuron copies and download all data saved in JSON format, respectively. Analogously, all data for correctly classified neuron copies can be downloaded as a JSON file.

small size of the dataset labeled as interneurons. To overcome the problem associated with a limited amount of data for the interneurons class, we extended this dataset with the A-GLIF interneurons models implemented in [17].[4] In this way the resulting training set included 58 labeled data for the pyramidal neurons and 50 data for the interneurons (instead of the initially 26). We found that in this case GBT had an accuracy of 80.3% and a precision of 0.927 for the pyr class and 0.679 for the int class. Fig. 15 depicts the confusion matrix for GBT trained with the experimental data for pyramidal neurons and experimental and A-GLIF data for the interneurons.

For each copy, we calculated the probability according to which it was classified as a member of one of the two classes. Then, we computed the mean ± standard deviation for all the neuron copies correctly classified as pyr and int. In this context, "correctly" should be intended as "as expected by the generation procedure", where a pyr/int copy which fires within the experimental regions computed by the algorithm is assumed to be pyr/int. These results suggest that it is possible to successfully classify a neuron copy as belonging to the class of pyramidal neurons or interneurons with an accuracy well above chance. Interestingly, the classification is highly accurate in terms of the probability with which each neuron copy is correctly assigned to a class (about 0.95 ± 0.08 for pyr and 0.94 ± 0.11 for int).

Fig. 13 shows a snapshot of the user interface for entering the required information and to visualize the resulting plots of the spike

[4] In [17] we proved the statistical indistinguishability of these models with the experimental data relative to the neuronal activity of interneuron cells. However, only for 24 interneurons the corresponding A-GLIF models are admissible, i.e. the resulting spike times at each stimulation current fall within the experimental region.

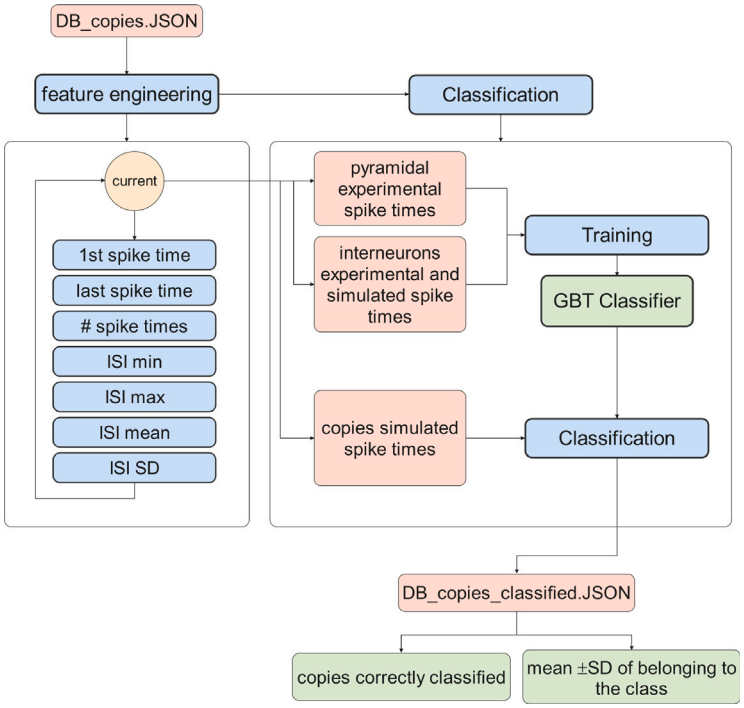

Fig. 14. Flow-chart illustration of the numerical implementation for the generation of a database of neuron copies classified.

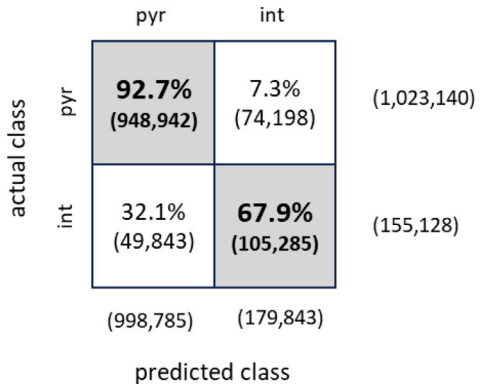

Fig. 15. Confusion matrix.

number as a function of the time for the copies that were correctly classified. All generated data can be downloaded as a JSON file.

4. Discussion

Integrate and fire-type models (IF), introduced more than a century ago by Lapique in [34], can be considered the first attempt to mathematically model a neuron's activity in response to an external input. The basic idea was so insightful that it brilliantly passed the proof of time, being still largely used in large-scale simulations of neural networks, due to computational efficiency and ability to retain the essential features of neuronal excitability. However, it soon became clear that neurons have much more complex dynamics, which need additional elements to be added to the simple IF scheme. As soon as it was experimentally and mathematically realized that transmembrane ion channels are the basic elements modulating neuronal response [35], different inward and outward ion currents, and their interplay, were found to underlie firing rate adaptation and other complex firing patterns in physiological and pathological conditions (e.g. [36–40]). The simple IF model thus needs to be extended to include at least two additional elements, representing the effect of inward and outward currents. As discussed in the Introduction, over the past years there have been several suggestions on how to consider these currents. In the model used for this work, which we called A-GLIF [17], the adaptation current I_{adap} represents outward currents, causing a hyperpolarizing effect, whereas the current I_{dep} represents inward currents, which generate a depolarization. Their concurrent dynamic makes the model able to a priori reproduce several electrophysiological features. However, it must be noted that a direct link between these currents and those generated by the plethora of ion channels cannot be established, since any IF models and their generalized variations still remain a system of linear ODEs.

The major limitation of the model, shared with any other model based on an IF scheme with a system of linear ODEs, is that it cannot reproduce the intrinsic complex dynamics observed in some neurons, and it cannot be directly linked to the biological/biochemical processes in effect in a real neuron. However, any short term modulatory effect, such as intracellular calcium dynamics, can be readily reproduced through its action on the spike times. In its current form, our model is able to reproduce all the different types of firing patterns of CA1 pyramidal neurons and interneurons. Other firing behaviors such as chattering or bistability (e.g. see Fig. 2 of [41]) were outside the scope of this work, and could be considered in future A-GLIF implementations of other neuron types. It is sufficient to note here that, for example, the model can be adapted to reproduce chattering during the optimization phase, by exploiting the monotonic dependence of the membrane potential V on the adaptation current I_{adap} and resetting I_{adap} to a large value after each burst, repeatedly applying the Monod block procedure.

In this work, we have introduced an automatic numerical procedure to generate neuron copies based on experimental and optimized data

Table S.1
Coefficients of the lower and upper limit curves for the region of experimentally feasible spike number y_{low}, y_{up}, respectively, as function of time t defined in Eq. (36), together with the largest time supporting a single spike for each constant stimulation current I_{stim} = 200, 400, 600, 800, 1000 pA, both for pyramidal neurons (upper table) and interneurons (lower table).

Pyramidal neurons					
	200 pA	400 pA	600 pA	800 pA	1000 pA
y_{low}	$\mathcal{J} = 1$ $\mathcal{D} = 0.004$ $\mathcal{F} = 1$ $\mathcal{G} = 0.333$ $t^1_{max} = 160$ ms	$\mathcal{J} = 1$ $\mathcal{D} = 0.005$ $\mathcal{F} = 1$ $\mathcal{G} = 0$ $t^1_{max} = 204.08$ ms	$\mathcal{J} = 1$ $\mathcal{D} = 0$ $\mathcal{F} = 0$ $\mathcal{G} = 0$ $t^1_{max} = 400$ ms	$\mathcal{J} = 1$ $\mathcal{D} = 9.6$ $\mathcal{F} = 0.08$ $\mathcal{G} = -13.0$ $t^1_{max} = 111.64$ ms	$\mathcal{J} = 1$ $\mathcal{D} = 190$ $\mathcal{F} = 0.008$ $\mathcal{G} = -195$ $t^1_{max} = 48.73$ ms
y_{up}	$\mathcal{J} = 0$ $\mathcal{D} = 0.27$ $\mathcal{F} = 0.6$ $\mathcal{G} = 0.5$ $t^1_{max} = 0$ ms	$\mathcal{J} = 0$ $\mathcal{D} = 0.5$ $\mathcal{F} = 0.6$ $\mathcal{G} = 0$ $t^1_{max} = 0$ ms	$\mathcal{J} = 0$ $\mathcal{D} = 0.28$ $\mathcal{F} = 0.7$ $\mathcal{G} = 1$ $t^1_{max} = 0$ ms	$\mathcal{J} = 0$ $\mathcal{D} = 0.3$ $\mathcal{F} = 0.69$ $\mathcal{G} = 1.1$ $t^1_{max} = 0$ ms	$\mathcal{J} = 0$ $\mathcal{D} = 0.33$ $\mathcal{F} = 0.7$ $\mathcal{G} = 1.1$ $t^1_{max} = 0$ ms
Interneurons					
	200 pA	400 pA	600 pA	800 pA	1000 pA
y_{low}	$\mathcal{J} = 1$ $\mathcal{D} = 0.011$ $\mathcal{F} = 1$ $\mathcal{G} = -0.286$ $t^1_{max} = 120$ ms	$\mathcal{J} = 1$ $\mathcal{D} = 0$ $\mathcal{F} = 0$ $\mathcal{G} = 0$ $t^1_{max} = 400$ ms	$\mathcal{J} = 1$ $\mathcal{D} = 0$ $\mathcal{F} = 0$ $\mathcal{G} = 0$ $t^1_{max} = 400$ ms	$\mathcal{J} = 1$ $\mathcal{D} = 12.05$ $\mathcal{F} = 0.1$ $\mathcal{G} = -17.5$ $t^1_{max} = 72.75$ ms	$\mathcal{J} = 1$ $\mathcal{D} = 0.011$ $\mathcal{F} = 1$ $\mathcal{G} = 0.556$ $t^1_{max} = 40$ ms
y_{up}	$\mathcal{J} = 0$ $\mathcal{D} = 1.3$ $\mathcal{F} = 0.428$ $\mathcal{G} = -1$ $t^1_{max} = 0$ ms	$\mathcal{J} = 0$ $\mathcal{D} = 0.14$ $\mathcal{F} = 1$ $\mathcal{G} = 3.2$ $t^1_{max} = 0$ ms	$\mathcal{J} = 0$ $\mathcal{D} = 0.2$ $\mathcal{F} = 1$ $\mathcal{G} = 3.0$ $t^1_{max} = 0$ ms	$\mathcal{J} = 0$ $\mathcal{D} = 0.22$ $\mathcal{F} = 1$ $\mathcal{G} = 4.0$ $t^1_{max} = 0$ ms	$\mathcal{J} = 0$ $\mathcal{D} = 0.135$ $\mathcal{F} = 1$ $\mathcal{G} = 5.0$ $t^1_{max} = 0$ ms

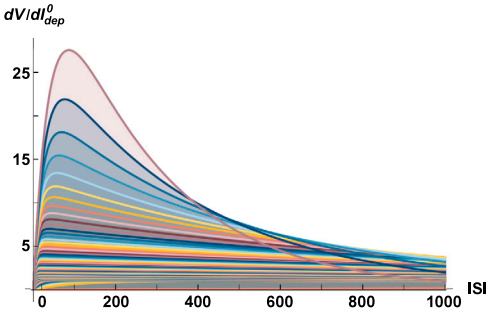

Fig. S.1. Plot of the derivative (26) as function of $t - t_0$ obtained imposing the conditions (13) with a step of 0.01 for both parameters β and δ.

for CA1 pyramidal neurons and interneurons. Our method relies on the simulation of neuron firing dynamics by means of the A-GLIF modeling framework, because of its ability to effectively capture such dynamics (and being computationally efficient), and of its analytical properties (which allow to control the copies firing behavior).

The neuron copies can be obtained by varying the 12 parameters of any given optimized model via scaling factors which, through a validation procedure, ensure that their firing properties remain within the observed experimental ranges. The parameters which can be potentially modified here are the initial conditions relative to the A-GLIF Cauchy problems (3 parameters), the Monod parameters defining the update value of the adaptation current (2 parameters), the firing blocks parameters determining the time interval in which the Monod function should be defined (6 parameters), and the internal nondimensional parameter α. These alterations lead to changes in both the spike times and the number of spikes, as summarized in Table 2.

The generation procedure introduced here allows to obtain an arbitrarily large number of heterogeneous neuron copies with a predictable dynamical behavior and falling within the experimental ranges of CA1 pyramidal neurons and interneurons. We provide approximately 1.2 millions (more precisely 1,178,268) predetermined copies (including the computed spike times) in a JSON database which can be downloaded from the *live paper section of EBRAINS* (see Fig. 13). Among these, 1,054,227 copies (approximately 89% of the total) are correctly classified as pyramidal neurons/interneurons.

In principle, other methods to generate copies can be implemented based, for example, on a random search of the entire parameter space. However, this type of approach would more easily result in the majority of copies producing unphysiological firing patterns. We have preferred to use a more conservative approach in which we perturbed individual parent optimizations in a controlled manner, ensuring a much more reliable implementation of copies.

Further experimental data, also related to other types of neurons, will allow us, in the future, to broaden such database and extend our approach to construct neural networks for different brain areas as well.

Supporting information

S1 Fig. Plot of the derivative of V with respect to I^0_{dep}

S2 Fig. Spike number as function of time for the pyramidal cell 95912006 on varying I^{start}_{adap}.

S3 Fig. Spike number as function of time for the pyramidal cell 95817008 on varying η

S4 Fig. Plot of the Monod functions for the pyramidal cell 95824006 on varying the parameter η.

S5 Fig. Plot of the Monod functions for the pyramidal cell 95824006 on varying the parameter c

S6 Fig. Spike number as function of time for the pyramidal cell 95817008 on varying c

S7 Fig. Number of spikes as function of the constant stimulation currents

S8 Fig. Spike number as function of time for the interneuron 99111001 on varying different parameters

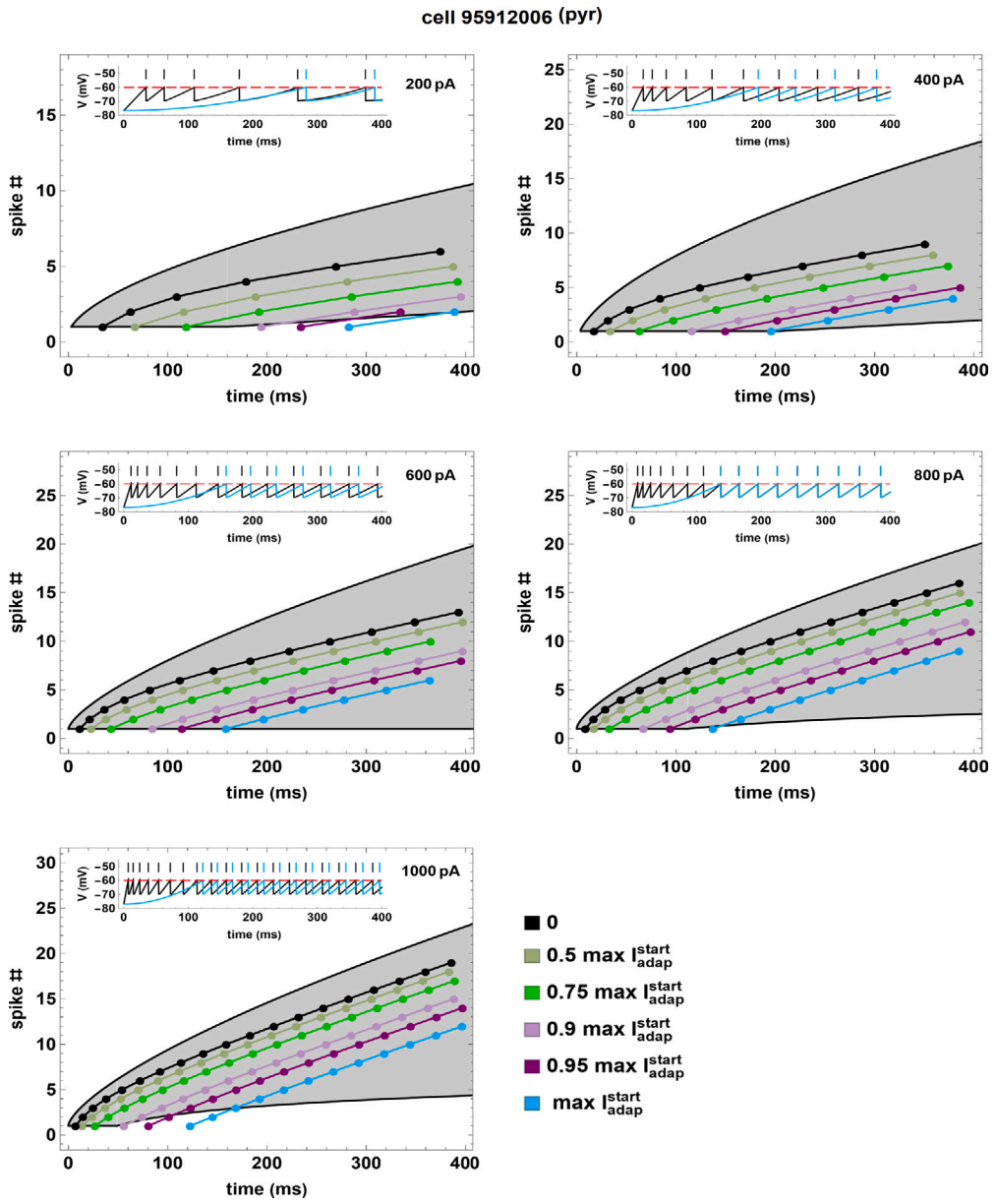

Fig. S.2. Spike number as a function of time for the pyramidal cell 95912006 (black curves and dots) and for 5 neuron copies (colored curves and dots) obtained by fixing the numerical values of all parameters except $I_{\text{adap}}^{\text{start}}$. For each current I_{stim} we set $\max I_{\text{adap}}^{\text{start}} = \alpha/\beta + I_{\text{dep}}^{\text{start}}(I_{\text{stim}} - I_{\text{th}})\theta(I_{\text{stim}} - I_{\text{th}})$. The gray areas cover the experimental regions of the data. The inset in each panel represents the original simulation of the firing dynamics compared with the copy corresponding to the $\max I_{\text{adap}}^{\text{start}}$.

Temporal shift of all spikes at nondimensional level

We consider variations in the dimensional parameters C_m, k_2, k_1, and τ_m (whose values are again derived from optimization procedures) such that α, β, and δ remain constant. Moreover, we adopt the same notation of Section 3.1.3 regarding "*old*" and "*new*" parameter values.

In this case, we assume $C_m^n = \frac{C_m^o}{p}$, $k_1^n = p\,k_1{}^\circ$, $k_2^n = p\,k_2{}^\circ$, and $\tau_m^n = \frac{\tau_m^o}{p}$, leading to $\tau^n = \frac{\tau^o}{p}$ while α, β, and δ do not change. Therefore, in this scenario the threshold current I_{th} also remains constant. This implies that both the stability conditions (13) and the conditions in Eq. (14) are automatically verified. In this scenario, the sole variation of the copies firing dynamics lies in the (nondimensional) ISIs as follows:

1. for $p < 1$ we have $\tilde{t}^n = \frac{p\,t}{\tau^o} < \tilde{t}^o$, therefore the (nondimensional) temporal dynamics are shrinking;
2. for $p > 1$ we have $\tilde{t}^n = \frac{p\,t}{\tau^o} > \tilde{t}^o$, therefore the (nondimensional) temporal dynamics are dilating.

We remark that the changes on τ outlined above only affect the nondimensional time scalings; consequently, although they might lead in the case $p < 1$ to a reduced computational cost to reproduce the same firing patterns of the original neuron, they will leave the curves corresponding to dimensional firing dynamics unaffected .

A priori validation for the perturbation of $\max I_{\text{adap}}^{\text{start}}$ *and* $I_{\text{dep}}^{\text{start}}$

The procedure mentioned in Section 3.2 is based on pre-selecting at least 4 scaling factors for the corresponding parameter, according to which the first spike time is calculated. This allows us to construct an interpolating function by associating coefficient values to their corresponding time of first spike. Taking into account the experimental boundaries available for each stimulation current, it is possible to identify the range of admissibility values for the parameter scaling factors (see Supp. Fig. S.9). These bounds are defined as piecewise

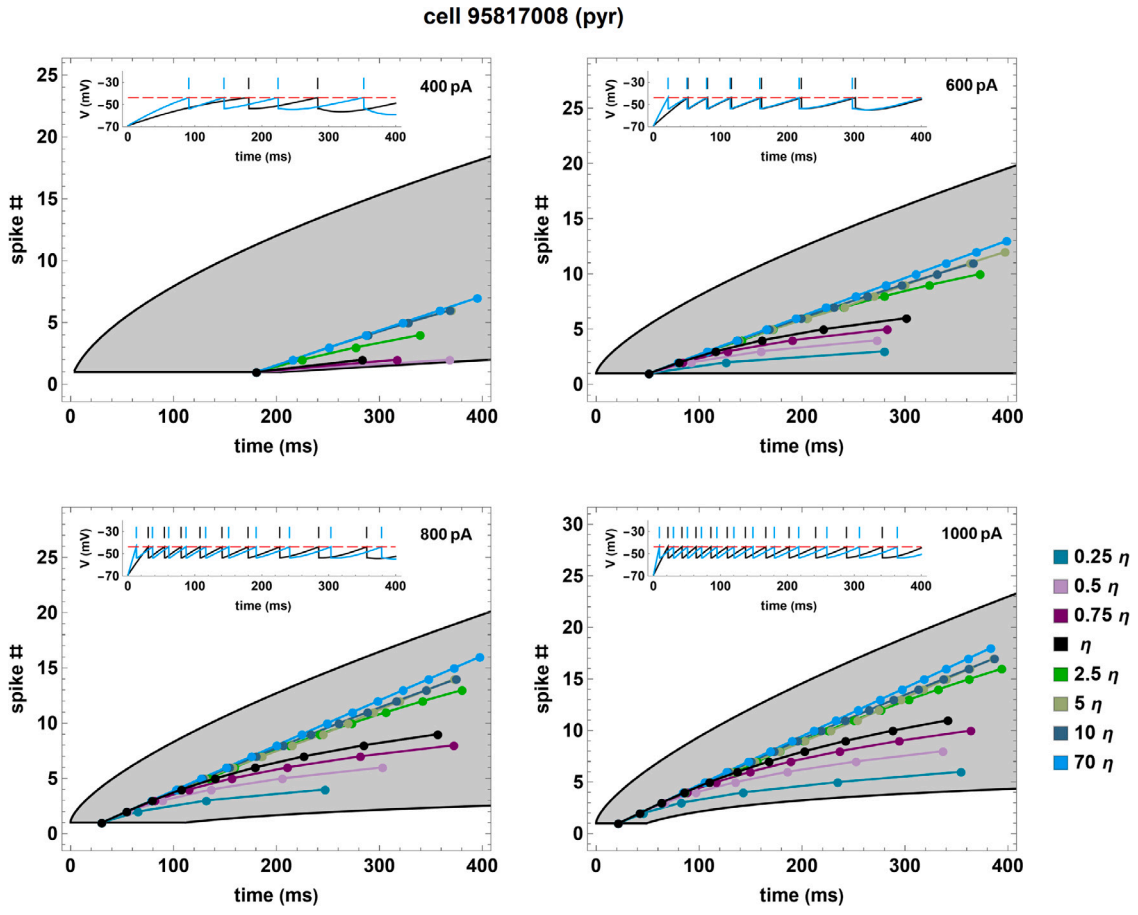

Fig. S.3. Spike number as a function of time for the pyramidal cell 95817008 (black curves and dots) and for 7 neuron copies (colored curves and dots) obtained by fixing all parameters except η in the Monod function (16). The inset in each panel represents the original simulation compared with the copy corresponding to $70\,\eta$.

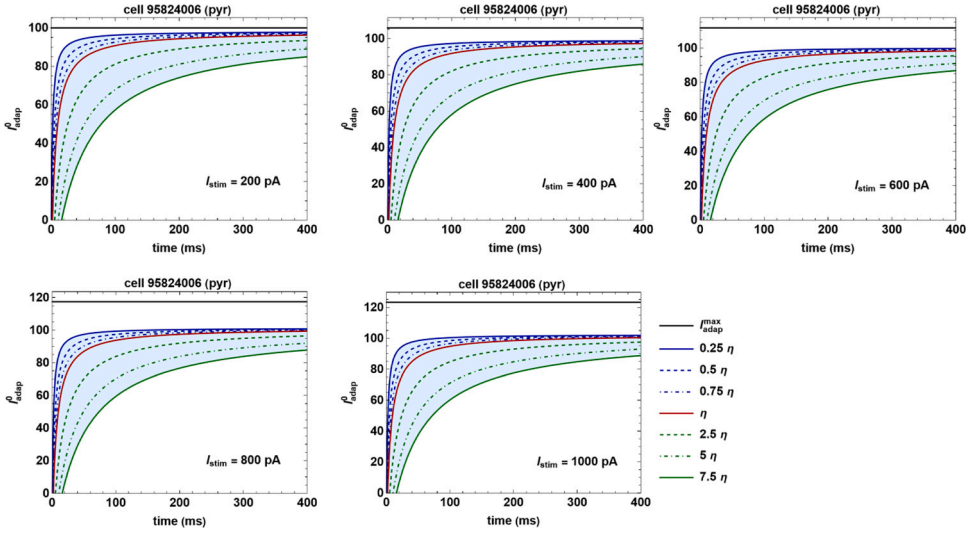

Fig. S.4. Plots of the Monod function (16) for the pyramidal cell 95824006 (red) and for the perturbed functions (blue and green) obtained on varying the parameter η. For each I_{stim} we set $I^{max}_{adap} = \frac{\alpha}{\beta} + I^0_{dep} + \frac{\delta}{\beta}(1 + V^0)$. In all cases $a > 0$.

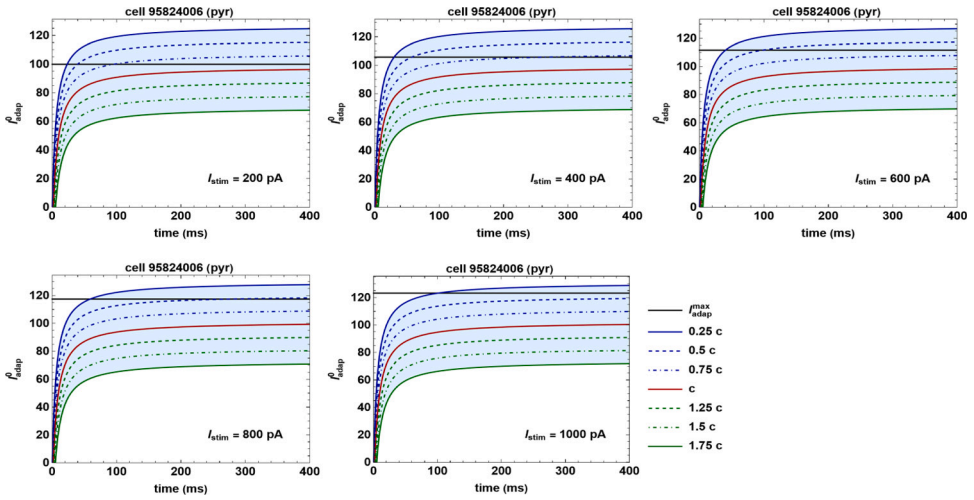

Fig. S.5. Plots of the Monod function (16) for the pyramidal cell 95824006 (red) and for the perturbed functions (blue and green) obtained on varying the parameter c. For each I_{stim} we set $I_{\text{adap}}^{\max} = \frac{\alpha}{\beta} + I_{\text{dep}}^{0} + \frac{\delta}{\beta}(1 + V^{0})$. In all cases $a > 0$.

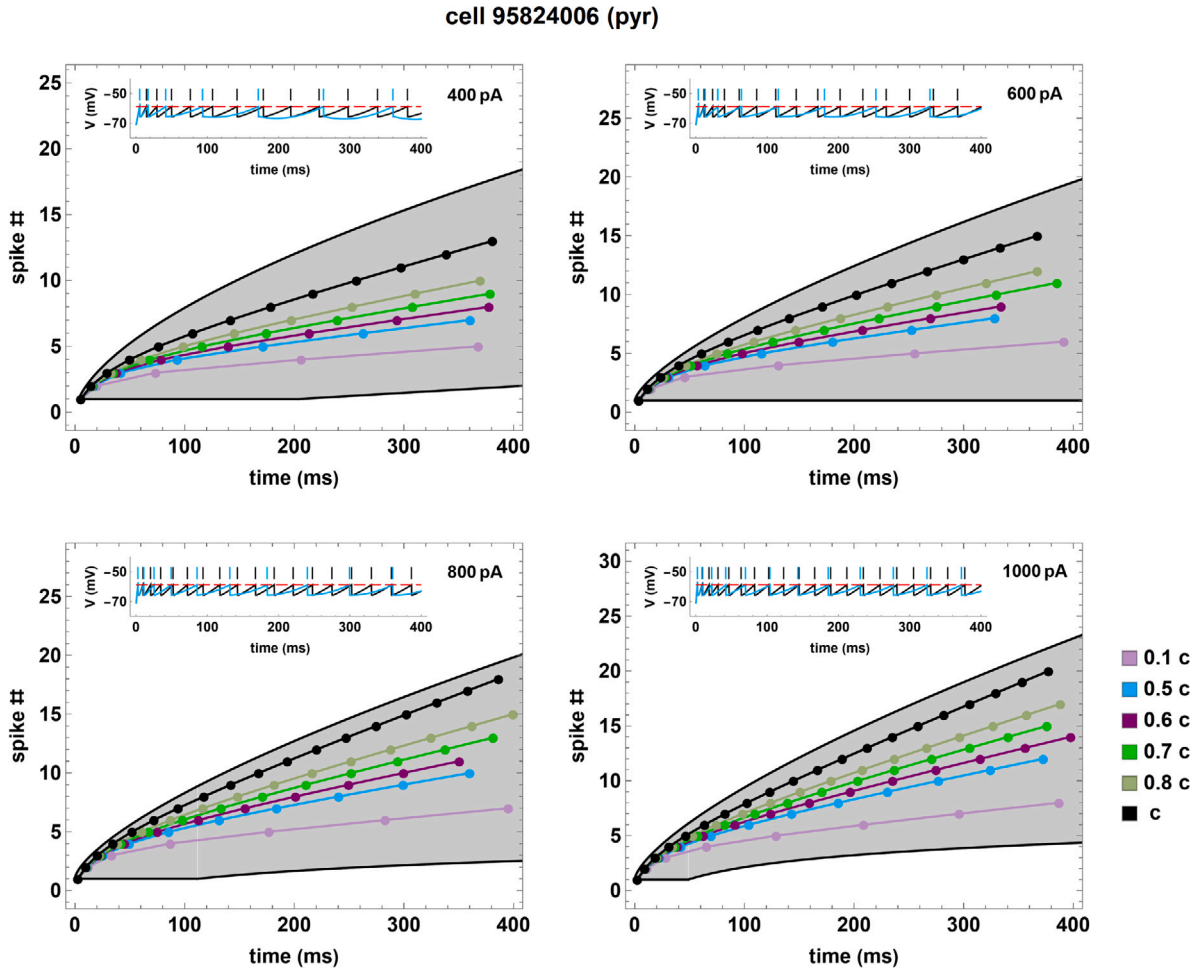

Fig. S.6. Spike number as a function of time for the pyramidal cell 95824006 (black curves and dots) and for 6 neuron copies (colored curves and dots) obtained by fixing all parameters except for c in the Monod function (16). The inset in each panel represents the original simulation compared with the copy corresponding to $0.5\,c$.

curves

$$y = \begin{cases} \mathcal{J} & \text{if } 0 \le t \le t^{1}_{\max}, \\ \mathcal{D}\,t^{\mathcal{F}} + \mathcal{G} & \text{if } t^{1}_{\max} < t \le 400 \text{ ms}, \end{cases} \tag{36}$$

where y represents the number of spike, t the time, and $t^{1}_{\max}(I_{\text{stim}})$ is the largest time supporting a single spike for the constant stimulation current I_{stim}.

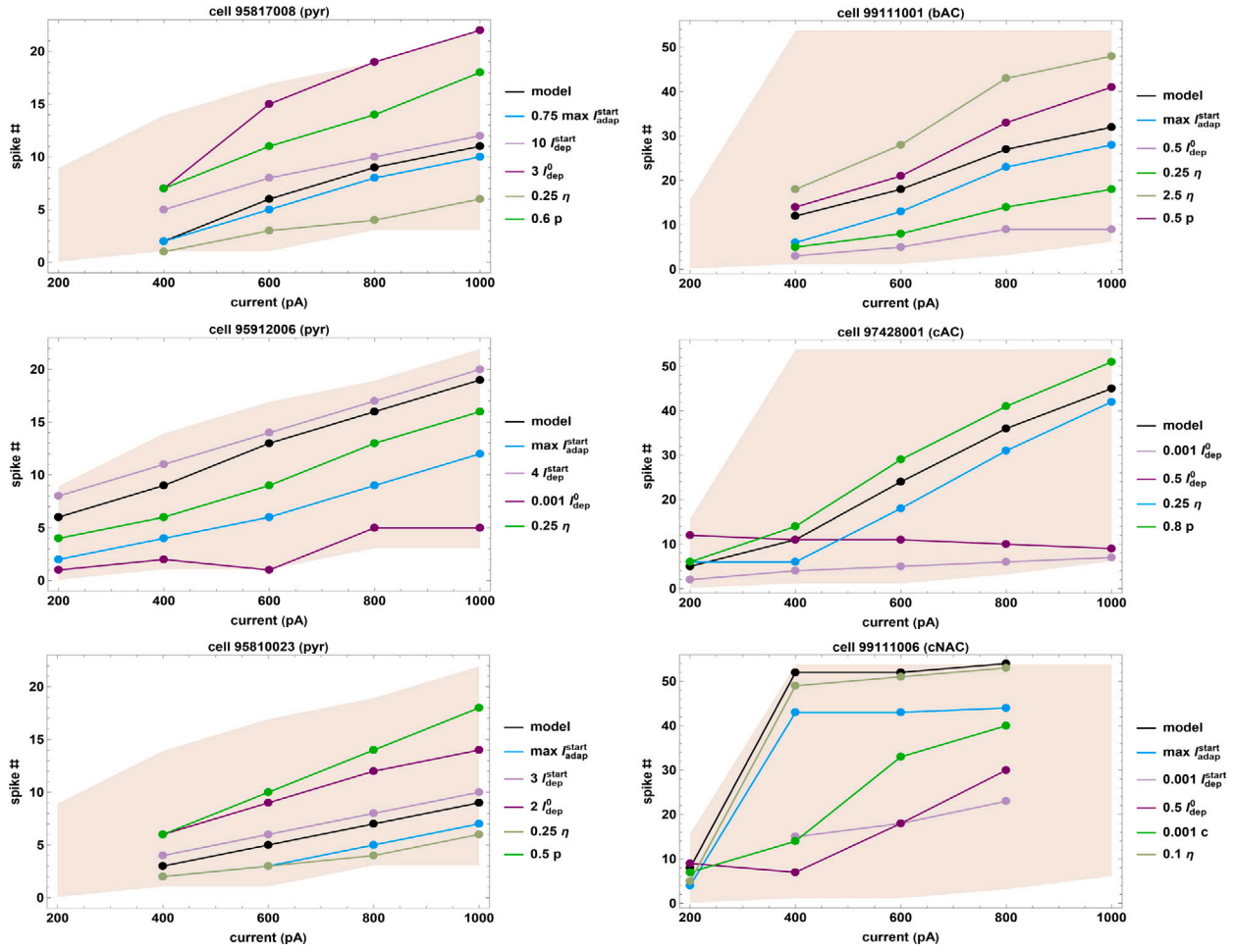

Fig. S.7. Number of spikes as function of different constant currents (black curves and dots) for three pyramidal neurons (left column) and three interneurons of bAC, cAC and cNAC type (right column, top, middle, and bottom, respectively) and for some copies (colored curves and dots) obtained by fixing the numerical values of all parameters except the ones indicated in the legends.

In particular, y_{low} (resp. y_{up}) is the curve bounding the experimental region from below (resp. above) in the space of spike numbers vs time. The values of the coefficients $\mathcal{J}$, $\mathcal{D}$, $\mathcal{F}$, $\mathcal{G}$, together with $t^1_{\max}(I_{\text{stim}})$, are provided in Table S.1. The final interval of admissibility for $\max I^{\text{start}}_{\text{adap}}$ and $I^{\text{start}}_{\text{dep}}$ is then obtained by intersecting the intervals related to the different constant stimulation currents considered. We note that the admissibility ranges for $\max I^{\text{start}}_{\text{adap}}$ and $I^{\text{start}}_{\text{dep}}$ vary for each reference neuron we use for the copies generation procedure.

Code availability. All model and simulation files will be available in the live papers section of EBRAINS (https://live-papers.brainsimulation.eu/).

CRediT authorship contribution statement

A. Marasco: Conception and design of the study, Developed the theoretical formalism, Performed the mathematical analysis, Writing – original draft. **C. Tribuzi:** Developed the software, Performed the data analysis, Writing – original draft. **A. Iuorio:** Developed the theoretical formalism, Performed the mathematical analysis, Writing – original draft. **M. Migliore:** Conception and design of the study, Writing – original draft.

Declaration of competing interest

All the authors declare that no competing interests exist.

Data availability

The code will be made available on request.

Acknowledgments

We thank Vittorio De Falco for the support in the initial stages of the code implementation. A.M. and A.I. acknowledge membership of the INdAM-GNFM Group. The authors also would like to thank Carmen Alina Lupascu for helpful feedback and support for the classification analysis, and Alessia Bonafede for technical and administrative assistance.

Funding

This paper has been funded by the EU Horizon Europe Program under the specific Grant Agreement 101147319, EBRAINS 2.0 project, and by a grant from the Swiss National Supercomputing Centre (CSCS) under projects ID ich002 and ich011, and FWF Hertha Firnberg Research Fellowship grant T 1199-N. We also acknowledge a contribution from the Italian National Recovery and Resilience Plan (NRRP), M4C2, funded by the European Union – NextGenerationEU (Project IR0000011, CUP B51E22000150006, "EBRAINS-Italy").

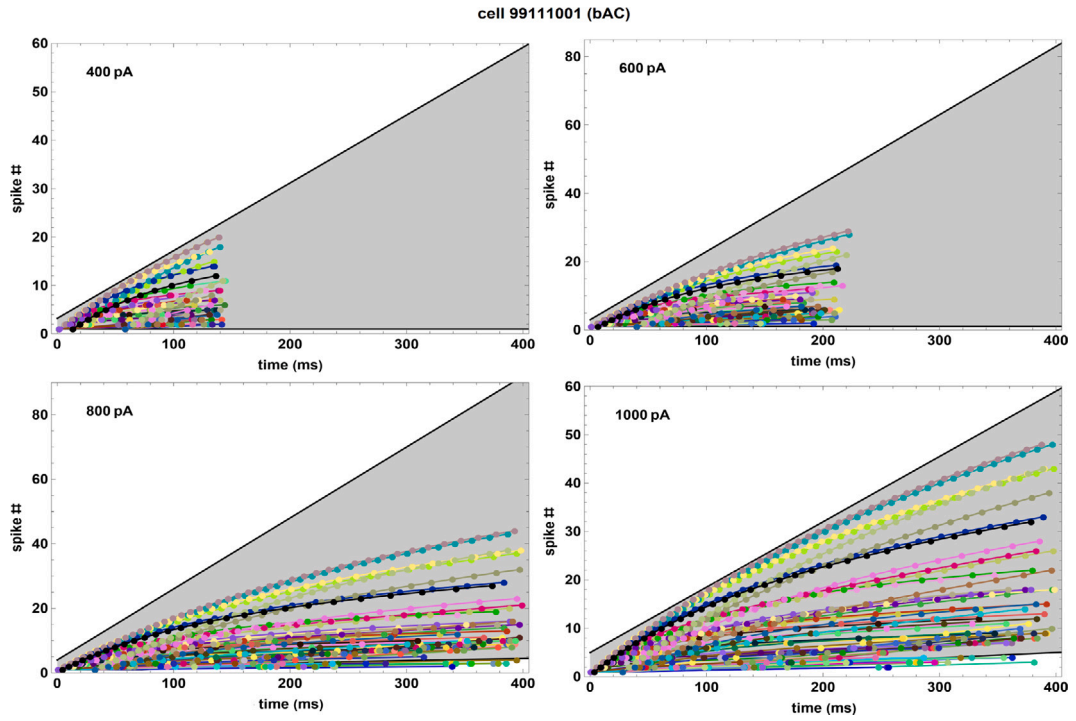

Fig. S.8. Spike number as a function of the spike times for the interneuron 99111001 (black curves and dots) and for 108 neuron copies (colored curves and dots) obtained from the former by varying the parameters as follows: h max $I_{\text{adap}}^{\text{start}}$ where $h = 0, 1$; $m\, I_{\text{dep}}^{\text{start}}$, where $m = 1, 10$; $n\, I_{\text{dep}}^{0}$ where $n = 0.001, 0.5, 1$; $p\, c$ where $p = 0.1, 1, 4$; $q\, \eta$ where $q = 0.25, 1, 2.5$. The original model is obtained by setting $h = 0, m = n = p = q = 1$ (black curves and dots).

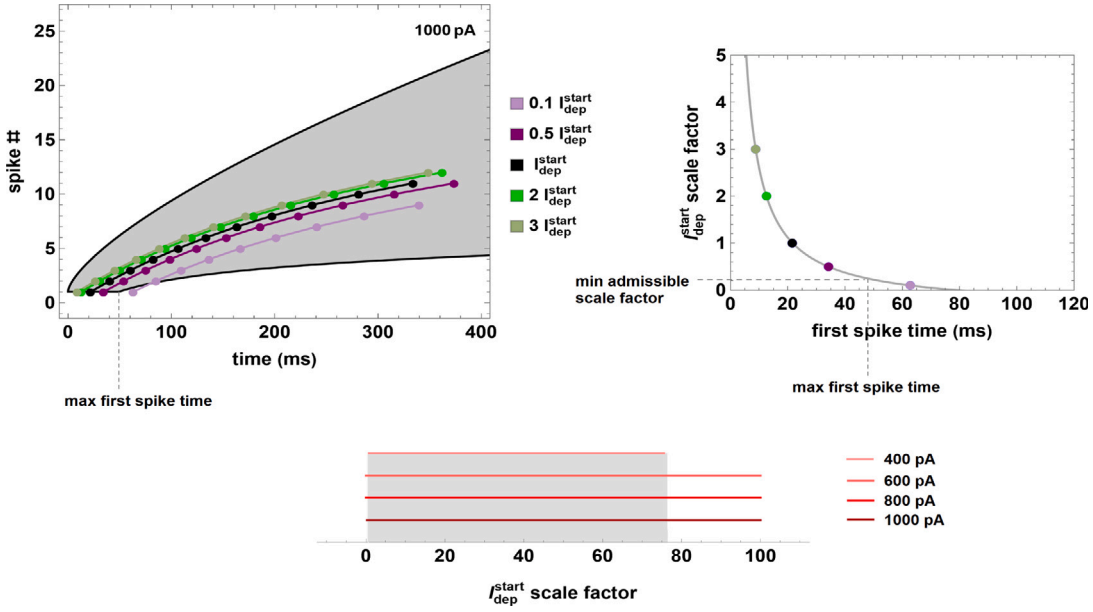

Fig. S.9. A priori validation procedure for the admissible range of the scale factors for $I_{\text{dep}}^{\text{start}}$. Top: (left) spike number as a function of the spike times at a current of 1000 pA for the pyramidal cell 95817008 (black curves and dots) and for 4 neuron copies (colored curves and dots) obtained by fixing the numerical values of all parameters except $I_{\text{dep}}^{\text{start}}$; (right) determination of the range of admissible scale factors for $I_{\text{dep}}^{\text{start}}$ for the stimulation current of 100pA. Bottom: determination of the range of admissible scale factors for $I_{\text{dep}}^{\text{start}}$ valid for all stimulation currents.

References

[1] Michael Breakspear, Dynamic models of large-scale brain activity, Nature Neurosci. 20 (3) (2017) 340–352.

[2] Matteo di Volo, Alberto Romagnoni, Cristiano Capone, Alain Destexhe, Biologically realistic mean-field models of conductance-based networks of spiking neurons with adaptation, Neural Comput. 31 (4) (2019) 653–680.

[3] Alberto Ferrara, David Angulo-Garcia, Alessandro Torcini, Simona Olmi, Population spiking and bursting in next-generation neural masses with spike-frequency adaptation, Phys. Rev. E 107 (2) (2023) 024311.

[4] F. Tesler, N. Tort-Colet, D. Depannemaecker, M. Carlu, A. Destexhe, Mean-field based framework for forward modeling of LFP and MEG signals, Front. Comput. Neurosci. 16 (2022).

[5] A.G. Giannari, A. Astolfi, Model design for networks of heterogeneous Hodgkin–Huxley neurons, Neurocomputing 496 (2022) 147–157.

[6] Henry Markram, Eilif Muller, Srikanth Ramaswamy, Michael W. Reimann, Marwan Abdellah, Carlos Aguado Sanchez, Anastasia Ailamaki, Lidia Alonso-Nanclares, Nicolas Antille, Selim Arsever, et al., Reconstruction and simulation of neocortical microcircuitry, Cell 163 (2) (2015) 456–492.

[7] Michele Migliore, Francesco Cavarretta, Michael L. Hines, Gordon M. Shepherd, Functional neurology of a brain system: a 3D olfactory bulb model to process natural odorants, Funct. Neurol. 28 (3) (2013) 241–243.

[8] Cheng Ly, Firing rate dynamics in recurrent spiking neural networks with intrinsic and network heterogeneity, J. Comput. Neurosci. 39 (3) (2015) 311–327.

[9] Tadashi Yamazaki, Jun Igarashi, Realtime cerebellum: A large-scale spiking network model of the cerebellum that runs in realtime using a graphics processing unit, Neural Netw. 47 (2013) 103–111.

[10] Eugene M. Izhikevich, Gerald M. Edelman, Large-scale model of mammalian thalamocortical systems, Proc. Natl. Acad. Sci. 105 (9) (2008) 3593–3598.

[11] Gabriel Marghoti, Thiago de Lima Prado, Arturo Cagnato Conte, Fabiano Alan Serafim Ferrari, Sergio Roberto Lopes, Intermittent chimera-like and bi-stable synchronization states in network of distinct Izhikevich neurons, Chaos Solitons Fractals 162 (2022) 112401.

[12] Eli Shlizerman, Konrad Schroder, J. Nathan Kutz, Neural activity measures and their dynamics, SIAM J. Appl. Math. 72 (4) (2012) 1260–1291.

[13] N.D. Jimenez, S. Mihalas, R. Brown, E. Niebur, J. Rubin, Locally contractive dynamics in generalized integrate-and-fire neurons, SIAM J. Appl. Dyn. Syst. 12 (3) (2013) 1474–1514.

[14] C. Teeter, R. Iyer, V. Menon, N. Gouwens, D. Feng, J. Berg, A. Szafer, N. Cain, H. Zeng, M. Hawrylycz, C. Koch, S. Mihalas, Generalized leaky integrate-and-fire models classify multiple neuron types, Nature Commun. 9 (1) (2018).

[15] Z. Wang, L. Guo, M. Adjouadi, A generalized leaky integrate-and-fire neuron model with fast implementation method, Int. J. Neural Syst. 24 (05) (2014) 1440004.

[16] A. Geminiani, C. Casellato, F. Locatelli, F. Prestori, A. Pedrocchi, E. D'Angelo, Complex dynamics in simplified neuronal models: Reproducing golgi cell electroresponsiveness, Front. Neuroinform. 12 (2018).

[17] A. Marasco, E. Spera, V. De Falco, A. Iuorio, C.A. Lupascu, S. Solinas, M. Migliore, An adaptive generalized leaky integrate-and-fire model for hippocampal CA1 pyramidal neurons and interneurons, Bull. Math. Biol. 85 (11) (2023) 1–39.

[18] Siva Venkadesh, Alexander O. Komendantov, Stanislav Listopad, Eric O. Scott, Kenneth De Jong, Jeffrey L. Krichmar, Giorgio A. Ascoli, Evolving simple models of diverse intrinsic dynamics in hippocampal neuron types, Front. Neuroinform. 12 (2018).

[19] Carlo R. Laing, The dynamics of networks of identical theta neurons, J. Math. Neurosci. 8 (1) (2018).

[20] A. Bandera, S. Fernández-García, M. Gómez-Mármol, A. Vidal, A multiple timescale network model of intracellular calcium concentrations in coupled neurons: Insights from ROM simulations, Math. Model. Nat. Phenom. 17 (2022) 11.

[21] Johannes Lengler, Florian Jug, Angelika Steger, Reliable neuronal systems: The importance of heterogeneity, PLoS One 8 (12) (2013) e80694.

[22] Yuanyuan Liu, Zhongkui Sun, Xiaoli Yang, Wei Xu, Dynamical robustness and firing modes in multilayer memristive neural networks of nonidentical neurons, Appl. Math. Comput. 409 (2021) 126384.

[23] Sima Mofakham, Michal Zochowski, Measuring predictability of autonomous network transitions into bursting dynamics, BMC Neurosci. 15 (S1) (2014).

[24] Nicolas Perez-Nieves, Vincent C.H. Leung, Pier Luigi Dragotti, Dan F.M. Goodman, Neural heterogeneity promotes robust learning, Nature Commun. 12 (1) (2021).

[25] Kestutis Pyragas, Augustinas P. Fedaravičius, Tatjana Pyragienė, Peter A. Tass, Entrainment of a network of interacting neurons with minimum stimulating charge, Phys. Rev. E 102 (1) (2020).

[26] Nathan W. Gouwens, Jim Berg, David Feng, Staci A. Sorensen, Hongkui Zeng, Michael J. Hawrylycz, Christof Koch, Anton Arkhipov, Systematic generation of biophysically detailed models for diverse cortical neuron types, Nature Commun. 9 (1) (2018).

[27] Divyansh Mittal, Rishikesh Narayanan, Resonating neurons stabilize heterogeneous grid-cell networks, eLife 10 (2021).

[28] Lida Kanari, Hugo Dictus, Athanassia Chalimourda, Werner Van Geit, Benoit Coste, Julian Shillcock, Kathryn Hess, Henry Markram, Computational synthesis of cortical dendritic morphologies, Cell Rep. 39 (1) (2022) 110586.

[29] Zeric Tabekoueng Njitacke, Sishu Shankar Muni, Soumyajit Seth, Jan Awrejcewicz, Jacques Kengne, Complex dynamics of a heterogeneous network of Hindmarsh-Rose neurons, 2022, arXiv preprint arXiv:2205.01790.

[30] Armando Romani, Felix Schürmann, Henry Markram, Michele Migliore, Reconstruction of the hippocampus, in: Advances in Experimental Medicine and Biology, Springer International Publishing, 2022, pp. 261–283.

[31] Shailesh Appukuttan, Luca L. Bologna, Felix Schürmann, Michele Migliore, Andrew P. Davison, EBRAINS live papers - Interactive resource sheets for computational studies in neuroscience, Neuroinformatics 21 (1) (2023) 101.

[32] Rosanna Migliore, Carmen A. Lupascu, Luca L. Bologna, Armando Romani, Jean-Denis Courcol, Stefano Antonel, Werner A.H. Van Geit, Alex M. Thomson, Audrey Mercer, Sigrun Lange, Joanne Falck, Christian A. Rössert, Ying Shi, Olivier Hagens, Maurizio Pezzoli, Tamas F. Freund, Szabolcs Kali, Eilif B. Muller, Felix Schürmann, Henry Markram, Michele Migliore, The physiological variability of channel density in hippocampal CA1 pyramidal cells and interneurons explored using a unified data-driven modeling workflow, PLOS Comput. Biol. 14 (9) (2018) e1006423.

[33] L.F. Abbott, P. Dayan, Theoretical Neuroscience Computational and Mathematical Modeling of Neural Systems, The MIT Press, 2001.

[34] L. Lapique, Recherches quantitatives sur l'excitation électrique des nerfs traitée comme une polarisation, J. Physiol. Pathol. Gen. 9 (1907) 620–635.

[35] A.L. Hodgkin, A.F. Huxley, A quantitative description of membrane current and its application to conduction and excitation in nerve, J. Physiol. 117 (4) (1952) 500–544.

[36] J.A. Connor, C.F. Stevens, Voltage clamp studies of a transient outward membrane current in gastropod neural somata, J. Physiol. 213 (1) (1971) 21–30.

[37] D.A. McCormick, J.R. Huguenard, A model of the electrophysiological properties of thalamocortical relay neurons, J. Neurophysiol. 68 (4) (1992) 1384–1400, PMID: 1331356.

[38] R.D. Traub, R. Llinas, Hippocampal pyramidal cells: Significance of dendritic ionic conductances for neuronal function and epileptogenesis, J. Neurophysiol. 42 (2) (1979) 476–496, PMID: 422974.

[39] Roger D. Traub, Robert K.S. Wong, Cellular mechanism of neuronal synchronization in epilepsy, Science 216 (4547) (1982) 745–747.

[40] X.-J. Wang, Multiple dynamical modes of thalamic relay neurons: Rhythmic bursting and intermittent phase-locking, Neuroscience 59 (1) (1994) 21–31.

[41] A.V.M. Herz, T. Gollisch, C.K. Machens, D. Jaeger, Modeling single-neuron dynamics and computations: A balance of detail and abstraction, Science 314 (5796) (2006) 80–85.